Hydrochemical mercury distribution and air-sea exchange over the submarine hydrothermal vents off-shore Panarea Island (Aeolian arc, Tyrrhenian Sea)

E. Bagnato[a,*], E. Oliveri[b], A. Acquavita[c], S. Covelli[d], E. Petranich[d], M. Barra[e], F. Italiano[f], F. Parello[g], M. Sprovieri[b]

[a] Dipartimento di Fisica e Geologia, Università degli Studi di Perugia, Via A. Pascoli, s.n.c., 06123 Perugia, Italy
[b] Istituto per l'Ambiente Marino Costiero, Consiglio Nazionale delle Ricerche (IAMC-CNR), Via del Mare 3, 91021, Torretta Granitola, Mazara, Trapani, Italy
[c] Agenzia Regionale per la Protezione dell'Ambiente del Friuli Venezia Giulia (ARPA-FVG), Via Cairoli, 14, Palmanova, Italy
[d] Dipartimento di Matematica e Geoscienze (DMG), Università degli Studi di Trieste, Via Weiss 2, 34127 Trieste, Italy
[e] Istituto per l'Ambiente Marino Costiero, Consiglio Nazionale delle Ricerche (IAMC-CNR), Calata Porta di Massa, 80133, Napoli, Italy
[f] Istituto Nazionale di Geofisica e Vulcanologia (INGV), Via U. La Malfa 153, 90146 Palermo, Italy,
[g] Dipartimento di Scienze della Terra e del Mare (DiSTeM), Università degli Studi di Palermo, Via Archirafi 36, 90123 Palermo, Italy

ARTICLE INFO

Keywords:
Dissolved gaseous mercury
Mercury evasion
Air-sea exchange
Hydrothermal fluids
Panarea Island

ABSTRACT

There is a growing concern about the mercury (Hg) vented from submarine hydrothermal fluids to the marine surrounding and exchange of dissolved gaseous mercury (DGM) between the sea surface and the atmosphere. A geochemical survey of thermal waters collected from submarine vents at Panarea Island (Aeolian Islands, southern Italy) was carried out in 2015 (15–17th June and 17–18th November), in order to investigate the concentration of Hg species in hydrothermal fluids and the vertical distribution in the overlying water column close to the submarine exhalative area. Specific sampling methods were employed by Scuba divers at five submarine vents located along the main regional tectonic lines. The analysis of the hydrothermal fluids indicates a site-to-site variation, with filtered total mercury (FTHg) concentrations ranging from 1072 to 4711 pM, as a consequence of the gas bubbles partial dissolution. These results are three orders of magnitude higher than the FTHg concentrations found in the overlying seawater column (ranging from 5.3 to 6.3 pM in the mid waters), where the efficient currents and vertical mixing result in more dilution, and potentially rapid transfer of the dissolved gaseous Hg to the atmosphere. Dissolved gaseous mercury (DGM) and gaseous elemental mercury (GEM) were simultaneously measured and combined in a gas-exchange model to calculate the sea-air Hg^0 evasional flux. Based on the data of DGM (range: 0.05–0.22 pM) and atmospheric GEM (range: 1.7 ± 0.35–6.4 ± 2.6 ng m^{-3}), we argue that the surface seawater off Panarea is mostly supersaturated in dissolved elemental gaseous mercury compared to the atmosphere, with a sea-air Hg^0 net flux ranging from 0.7 to 9.1 ng m^{-2} h^{-1} (average: $\sim 4.5 \pm 3.5$ ng m^{-2} h^{-1}). Since the empirical gas-exchange model does not include the contribution of Hg^0 released as gas bubbles rising from the vents toward sea-surface, the calculated Hg^0 evasional flux for this location is most likely larger.

1. Introduction

There is general agreement in the scientific community that submarine hydrothermal activity exerts significant controls on the chemical composition of seawater, by providing major and trace-ions that have been leached from mantle rocks (Tivey, 2007; Von Damm et al., 1985). This process is particularly effective in the Mediterranean Sea, where coastal seawater is poorly flushed compared to that of other oceans, and most of the known submarine hydrothermal venting is from shallow water (depth < 200 m) (Dekov and Savelli, 2004). Even though these contributions seem to be of little importance on a global scale, hydrothermal submarine emissions may become significant locally representing hotspots for the occurrence of the accumulation dynamics of toxic trace metals along the trophic web (Andaloro et al., 2012; Asthakhov et al., 2005; Von Damm et al., 1985). Mercury (Hg) is known as a global pollutant, and is widespread in the environment (Schroeder and Munthe, 1998). The ocean plays an important role in the complex biogeochemical cycling of this element, because, once it is

* Corresponding author.
E-mail address: emu.bagnato@gmail.com (E. Bagnato).

Accepted 11 April 2017

in the aquatic environment, it can convert to methylmercury (MMHg) and bio-accumulates in the food chain (Morel et al., 1998; Fitzgerald et al., 2007; Mason and Sheu, 2002; Soerensen et al., 2010).

The consumption of fish with high MMHg levels can lead to adverse health effects in human beings and wildlife (USEPA, 1997). Closed marine water systems, such as the Mediterranean Basin, are very sensitive to Hg pollution due to the limited exchange of water with the oceans. Fish harvested from the Mediterranean Sea is an important part of the diet in the region. Data in the literature on Hg contamination reveal a more marked bioavailability in the Southern Tyrrhenian Sea, which is the easternmost and deepest part (about 3500 m) of the Western Basin, where submarine volcanic emissions represent a local source of relevance that can determine great Hg enrichments in sediment and biological species (Andaloro et al., 2012). The importance of submarine hydrothermal activity as a potential long-term supplier of Hg to the marine environment has also been emphasized by previous researches that report significant Hg accumulation in bottom sediments (Dekov, 2007; Astakhov et al., 2007; Prol-Ledesma et al., 2002; Cronan, 1972). To date, however, knowledge of the extent to which Hg is released from hydrothermal vents into the ocean and its impact on bioaccumulation has been elusive (Dekov, 2007; Prol-Ledesma et al., 2004). Generally, the hot hydrothermal fluids and gases rise up and mix with the entrained seawater concentrating and transporting Hg along the seawater column (Varekamp and Buseck, 1984; Krupp, 1988). The speciation of soluble Hg in hydrothermal fluids is dominated by disulfide complexes (i.e., $Hg(HS)_2^0$, $HgHS_2^-$, and HgS_2^{2-}) at a pH range of 4–8 in the presence of high levels of hydrogen sulfide ($\geq 10^{-2}$ mol kg^{-1}), as well as under moderately reducing conditions in fairly hot fluids (> 200 °C) (Krupp, 1988). Elemental mercury (Hg^0_{aq}) can also be transported in hydrothermal fluids as water plumes with low hydrogen sulphide concentrations ($\leq 10^{-4}$ mol kg^{-1}) under strongly reducing conditions (Krupp, 1988). Finally, transport of Hg in its elemental form as uncharged aqueous species Hg^0_{aq} may be also released from the fluids and vented to the atmosphere directly via CO_2-rich gas bubbles as dissolved gaseous mercury (Varekamp and Buseck, 1984). Conversely, Hg complexes of Cl^-, CO_3^{2-} and OH^- ligands have been demonstrated to be of no significance in the hydrothermal transport of Hg (Krauskopf, 1951; Barnes, 1979; Khodakovskiy and Shikina, 1983; Varekamp and Buseck, 1984).

In the current study, we investigated the concentration of Hg species in hydrothermal fluids and their vertical distribution in the overlying water column close to the submarine exhalative area 2.5 km offshore, east of Panarea Island (Aeolian archipelago). Visual observations and geochemical surveys were performed within the hydrothermal field that extends on the shallow seafloor from the main Island to the group of islets located to the northeast (Fig. 1).

There is still limited knowledge of the magnitude of the air-sea exchange mechanisms, which are one of the main factors affecting the overall uncertainty associated with the assessment of the net fluxes of Hg between the marine and the atmospheric environments in Mediterranean region. As a result, we propose an in-depth investigation of the production of the volatile DGM in the marine ecosystem and its subsequent transfer into the atmosphere as gaseous elemental mercury (GEM or Hg^0_g). These measurements, which are the first carried out at such a location: 1) extend the previous DGM records existing in literature for adjacent areas in the Mediterranean Sea (Caramanna et al., 2010; Andersson et al., 2007; Kotnik et al., 2007, 2013; Gardfeldt et al., 2003; Horvat et al., 2003; Lanzillotta and Ferrara, 2001); and 2) improve the poor understanding of the submarine hydrothermal discharging processes affecting Hg concentrations in the basin, to date.

2. Experimental method

2.1. Study area

The investigated submarine hydrothermal vents are located off the eastern coast of Panarea Island, which is a volcanic structure belonging to the archipelago of the Aeolian Arc (Tyrrhenian Sea, Italy) (Fig. 1). The most intense submarine emissions are located at the sea-bottom among five emerging reefs (Dattilo, Bottaro, Lisca Bianca, Panarelli and Lisca Nera) arranged along a circular rim that is about 1 km in diameter, representing the remnants of an ancient volcanic center (Italiano and Nuccio, 1991; Gabbianelli et al., 1986). The first geochemical surveys carried out since the early 1980s (Italiano and Nuccio, 1991; Inguaggiato and Italiano, 1998) revealed the existence of a deep hydrothermal system beneath a large field of submarine gas emissions located about 2.5 km east of the island. The deep geothermal reservoir at temperatures of 220–280 °C is superimposed by two different shallow submarine hydrothermal systems, one of which is partially recharged by continental waters from Panarea Island and the other by marine waters (Italiano and Nuccio, 1991). The two systems have temperatures of about 170–210 °C and feed the hydrothermal emissions on the seafloor. The recent submarine volcanic activity is characterized by the widespread presence of gas vents and hydrothermal seepages which are controlled by the NE-SW, NW-SE and N-S oriented fault-system that follows the dominant, regional, permeable tectonic lineaments of the Aeolian Islands (Italiano and Nuccio, 1991; Gasparini et al., 1982). The discharging fluids and gases rise up and mix with the entrained seawater producing chemically altered plumes (Fig. 2; Resing et al., 2004; Solomon et al., 2009) which strongly modify the environmental chemical-physical parameters (mainly pH), also promoting the dissolution of some benthic foraminiferal assemblages at some extent (Panieri et al., 2005). Besides, most of the hydrothermal emissions are often marked by white bacterial mats that appear as a white film of colloidal sulphur deposits containing numerous filaments of colourless sulphur-oxidizing bacteria (Gugliandolo et al., 2006) (Fig. 2).

2.2. Sample collection and handling

An intense geochemical survey was performed during two oceanographic cruises in 2015 (15–17th June and 17–18th November, respectively) on board the Italian Research Vessel (RV) *BioForYou* within the framework of the MONSOON (MONitoraggio SOttomarino per scopi ambientali ed energetici) Italian research program. Samples of dry and dissolved gas, thermal waters and the overlying seawater column were collected from five different hydrothermal emissions identified by scuba divers (Fig. 1). The selected vents, La Calcara (LC), Campo 7 (C7), Bottaro Crater (BC), Bottaro North (BN), and Black Point (BP), are relatively close to each other, and located between 8 and 23 m below sea level (Fig. 1). The sampling locations were selected according to earlier studies reported in the literature (Italiano and Nuccio, 1991; Caracausi et al., 2005; Gugliandolo et al., 2006). A control station (Field Blank; FB) characterized by a 25 m-bottom depth, located at about 3 km from the main discharging sites and 1 km from the LC site, does not have any gas vent and was chosen as a representative of ambient seawater that is not contaminated by hydrothermal activity (Fig. 1). All the sampling stations were georeferenced and localized on a cartographic map as reported in Fig. 1. Ultra-trace Hg clean techniques (USEPA, 2002) were applied during the entire cruise. A system made of a Teflon probe and a syringe connected by a three-way valve to a pre-cleaned Pyrex bottle was used to collect samples of thermal waters (i.e. hydrothermal fluids). The bottle stopper had two holes sealed by valves. The probe was introduced to the sea floor as deep as possible at each emission point in order to minimize the potential contamination by seawater. The entire sampling system was first filled by the hydrothermal gas to move out the seawater and keep the contamination level as low as possible. Consequently, by using the syringe, the thermal water was pumped into the glass bottle through one of the valves located on the stopper. Simultaneously, the same volume of gas was drawn out through the second valve and the procedure was repeated until the bottle was completely filled with thermal water (Fig. 2a,b). At each station, the sample was brought to the surface by keeping both the stopper valves

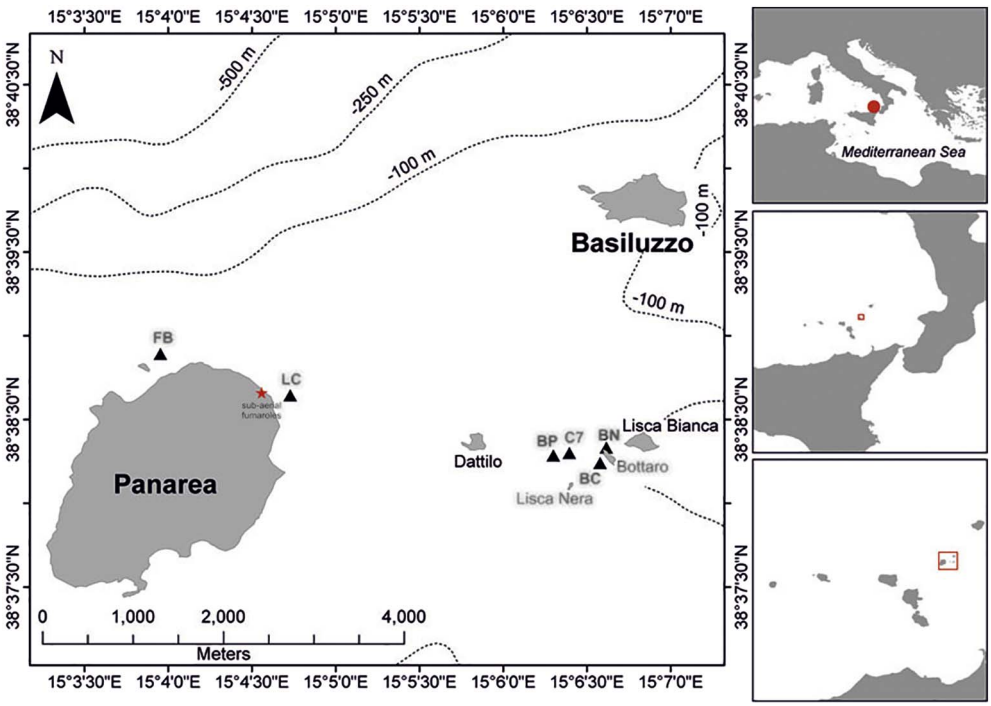

Fig. 1. Rough map of the investigated area east of the Panarea island. The islets of Dattilo, Bottaro, Lisca Bianca and Lisca Nera have been recognized as being the remnants of a crater rim. The sampling hydrothermal vent sites (BP: Black Point; LC: La Calcara; BN: Bottaro North; BC: Bottaro Crater; C7: Campo 7; FB: Field Blank) and the inland fumaroles (red star) are also reported.

closed (Italiano and Nuccio, 1991). Sampling of the water column was performed consecutively over each discharging vent to determine the spatial impact of the local hydrothermal emissions in the marine surroundings. Seawater samples were collected by scuba divers at three different depths of the column (surface, mid-water and bottom) using a single 10 l Niskin bottle equipped with silicon seals and springs. All the samples were preserved in bottles previously cleaned with HNO_3/HCl (10%) and rinsed with Milli-Q water (18.2 MΩ cm^{-1}). Onboard, the sample containers were rinsed three times by sample seawater prior to filling, while environmental parameters (T, pH and Eh) were immediately determined using portable electrodes (Crison MM 40 +). The samples were stored according to specific protocols used for examining mercury chemical speciation (Parker and Bloom, 2005) and determining standard major ions. The sampling of the thermal fluids and seawater was intended to estimate filtered total mercury (FTHg), divalent reactive mercury (RHg) and dissolved gaseous mercury (DGM).

2.3. Analytical methods

2.3.1. Geochemistry of hydrothermal vents

The analytical operations for the geochemistry determinations of the thermal waters and gases were all performed at the Istituto Nazionale di Geofisica e Vulcanologia, Sezione di Palermo (INGV-PA). The major dissolved ions in the hydrothermal fluids were analyzed using ion chromatography systems (1100 IC, Dionex) equipped with an anion column (AS14A) and a precolumn (AG14A) that works under

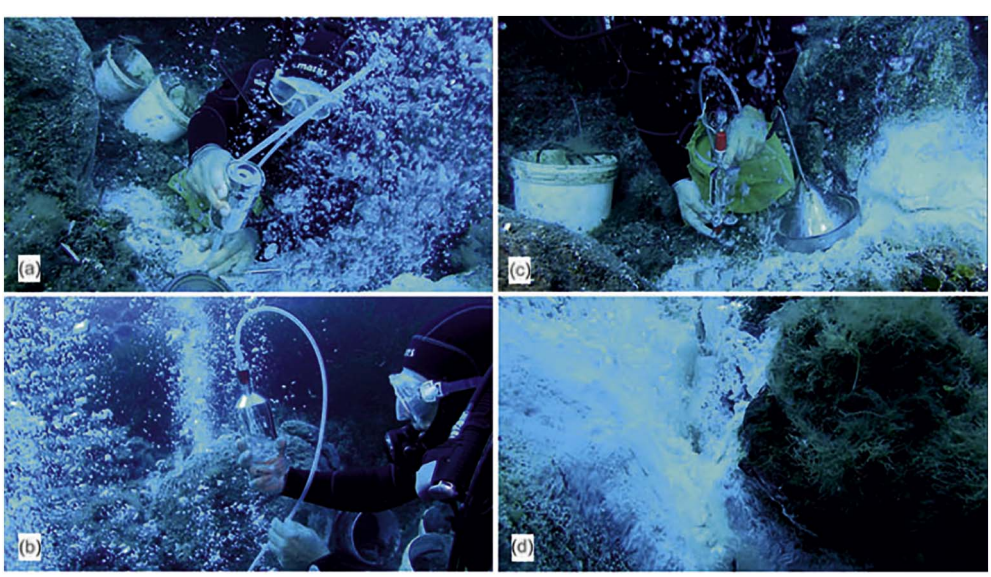

Fig. 2. Pictures illustrating the sampling of warm thermal waters (a,b) and dry gas phase (c) for mercury speciation and major chemical determinations. White bacterial mats deposits (d) often marks the submarine hydrothermal emissions at Panarea Island.

continuous flow of the carbonate–bicarbonate eluent, and a cation column (CS12A) and precolumn (CG12A) that works under continuous flow of methanesulfonic acid, while the total alkalinity was determined by the titration method once in the lab. These latter can be used just as indicative data, owing to the limits of our HCO^{3-} analysis. For what regards the gascromatographic analyses, the sample is introduced and split in two aliquots: one is analyzed with a Agilent 7890B with two columns in series (Poraplot U 25 m × 0.53 mm and Molsieve 5A 25 m × 0.53 mm) fluxed by Ar, detectors TDC and FID with methaniser. This aliquot is analyzed for He, H_2, O_2, N_2, CH_4 and CO. The other aliquot is analyzed for CO_2 and H_2S by a microGC module (MicroGC 3000) equipped with Poraplot U column (15 m) fluxed by He, detector TCD.

The $^3He/^4He$ as well as the $^4He/^{20}Ne$ ratios were measured by a Thermoscientific Helix SFT static mass spectrometer.

2.3.2. Filtered total mercury (FTHg)

Analyses of the Hg geochemistry were carried out at both Agenzia Regionale per la Protezione Ambientale (ARPA) and the Dipartimento di Matematica & Geoscienze (DMG), in Trieste. The seawater samples for the total Hg were filtered through cellulose filters (0.45 μm), oxidized (250 μl BrCl) and stored in ultra-clean washed Pyrex flasks to keep them dark and cold in double plastic zip-bags before the analyses. Once in the lab, the excess oxidizer was reduced with aqueous hydroxylammonium hydrochloride followed by the reduction of mercuric ions with the addition of a stannous chloride solution, according to the EPA method 1631 for ultra-trace Hg analysis in natural water (USEPA, 2002). The $Hg^0_{(g)}$ formed in the samples was purged with mercury free argon, collected on gold traps and analyzed by cold vapor atomic fluorescence spectrometry (CVAFS Mercur-Analytic Jena). Prior to the analyses, hydrothermal fluids were initially digested according to the DIN EN 1483 method in order to reduce the effect of the excess sulphur. After digestion, the reduction of mercuric ions in the thermal waters was accomplished according to the EPA method 1631 and analyzed by CVAFS.

2.3.3. Reactive dissolved mercury (RHg or Hg^{2+})

Divalent RHg determination includes dissolved inorganic Hg species, labile organo-Hg associations, and Hg that is readily leachable from any particulate matter present. In this study, the RHg was determined using the same apparatus (CVAFS). The only exception was that the fresh, un-acidified and un-oxidized samples were treated directly with $SnCl_2$ (Parker and Bloom, 2005) and analyzed a few days after collection. Generally, it is not possible to preserve samples for RHg determination, because the acidification quickly and dramatically alters the measured Hg^{2+} levels in unpredictable ways. Acidification can lead to either the desorption of Hg^{2+} from particulates or the oxidation of Hg^0 to Hg^{2+} (Parker and Bloom, 2005). As the analysis for the RHg determination was performed two days after collection, the storage time could not affect the data. The system for FTHg and RHg was calibrated by running a number of certificate standard solutions (NIST 3133). The detection limit (LOD) was estimated to be ~0.44 ng l^{-1} based on the three times standard deviation of the system blank.

2.3.4. Dissolved gaseous mercury (DGM)

The samples for DGM were collected underwater directly into a 0.5 L Pyrex glass flask by means of a silicon tube. Once in the geochemistry laboratory at IAMC-CNR (sez. Capo Granitola), the liquid samples were purged by a 300–400 ml min^{-1} flow of ultrapure N_2 for 10 min. Volatile Hg species were collected on specific sampling gold traps and then transferred to a CVAFS analyzer system supplied by the ARPA Institute, in Trieste. The DGM on the sampling gold trap was released by heating (500 °C) it for 1 min in a flow of argon to a permanent gold trap (heating for 1 min at about 500 °C), released again and detected by a CVAFS analyzer. The method is described in detail by Horvat et al. (2003) and Gardfeldt et al. (2003). Three blanks were prepared by conditioning the traps through the N_2 purge of 500 ml of ultrapure water. The method detection limit (MDL) was 0.004 pM, which was defined as three times the standard deviation of the blanks. The procedure blank equivalent concentration was 0.02 pM. These levels corresponded to < 10% of the concentrations found in both the hydrothermal and surface seawater samples.

2.3.5. Elemental mercury in bubbling gases

In order to collect Hg^0 in the dry gas phase (bubbles) of the hydrothermal discharge, a plastic funnel was inverted (30 cm diameter with some kilograms of ballast around the lower ring) and placed precisely on the gas vent to be sampled (Fig. 2c). The funnel was connected, through a silicon hose, to a Pyrex glass flask with twin valves. This flask was pre-filled with air at a pressure above that of the hydrostatic pressure expected at the sampling depth in order to stop seawater from entering the sampler (Italiano and Nuccio, 1991; Caramanna et al., 2005). The collection funnel was filled with the gas and the sampling glass flask was opened and allowed to reach equilibrium with the gas to be sampled. Once in the lab, the collected gaseous $Hg^0_{(g)}$ was then concentrated into specific gold traps and detected by the CVAFS technique. Simultaneously, estimates of the gas flow rate at each submarine fumarole were computed by connecting the funnel to a tank of a known volume. By counting the gas filling time, it was possible to calculate the flow rate (litres per minute) at any given vent. The filling time (seconds) was measured by filming the process using a high definition video camera (GoPro Hero2). The investigated fumaroles showed predominantly small degassing activity with gas flow rates ≤ 2 l/min, according to previous determinations made by Steinbruckner (2009).

2.3.6. Atmospheric gaseous elemental mercury (GEM) measurements

In the marine boundary layer overlying the submarine hydrothermal field of Panarea, the concentration of GEM was measured in real-time along a route chosen out of the main investigated discharging vent alignments (Fig. 3). The survey was carried out within the first half of a very sunny and warm day on 18th November 2015, and the main hydro-meteorological conditions did not change. During the survey, we measured an average seawater temperature of 20 °C (range from 18 to 22 °C) using a dedicated fiber-optic sensor; meanwhile a portable weather station (Xplorer 4 Skywatch) estimated a wind velocity of ~4 m s^{-1} and a mean air temperature of 23 °C. The analysis of the atmospheric GEM concentrations was performed using an automated real-time atomic adsorption spectrometer (Lumex-RA 915 M) in the standard monitoring mode (Sholupov et al., 2004). We sampled air at 1-s intervals by covering a total marine distance of about 3 km at a vessels speed of ~9 knots (about 16 km h^{-1}). Based on a three times standard deviation of the system blank, the gas analyzer has a detection limit of 2 ng m^{-3} at a sampling time of 1 s and a flow rate of 10 l min^{-1} (Sholupov et al., 2004) and an accuracy of 20% checked by annual testing by the manufacturer (LUMEX, St. Petersburg). The analyzer monitored the GEM concentrations using differential atomic absorption spectrometry with correction for background absorption via the Zeeman Effect (Sholupov et al., 2004). A zero correction resets the baseline every 5 min during sampling. This approach has been successfully used in various GEM measurements elsewhere (Ci et al., 2011; Bagnato et al., 2011; Kim et al., 2006), and showed good agreement with the conventional gold trap/CVAFS system (Aiuppa et al., 2007; Bagnato et al., 2014). During the cruise, the air was sampled 1 m above the topmost point of the deck of the vessel (~3 m above the sea level overall) at its bow. The vessel-induced contamination during motion was assumed to be minimal.

Additional atmospheric GEM measurements were performed closer to the sea-surface at about 1 m a.s.l., by stopping the vessel over each georeferenced vent, with the aid of a GPS, and by acquiring data through the Lumex analyzer for 10 min. This approach was aimed at reducing the atmospheric turbulence, which causes a reduction of

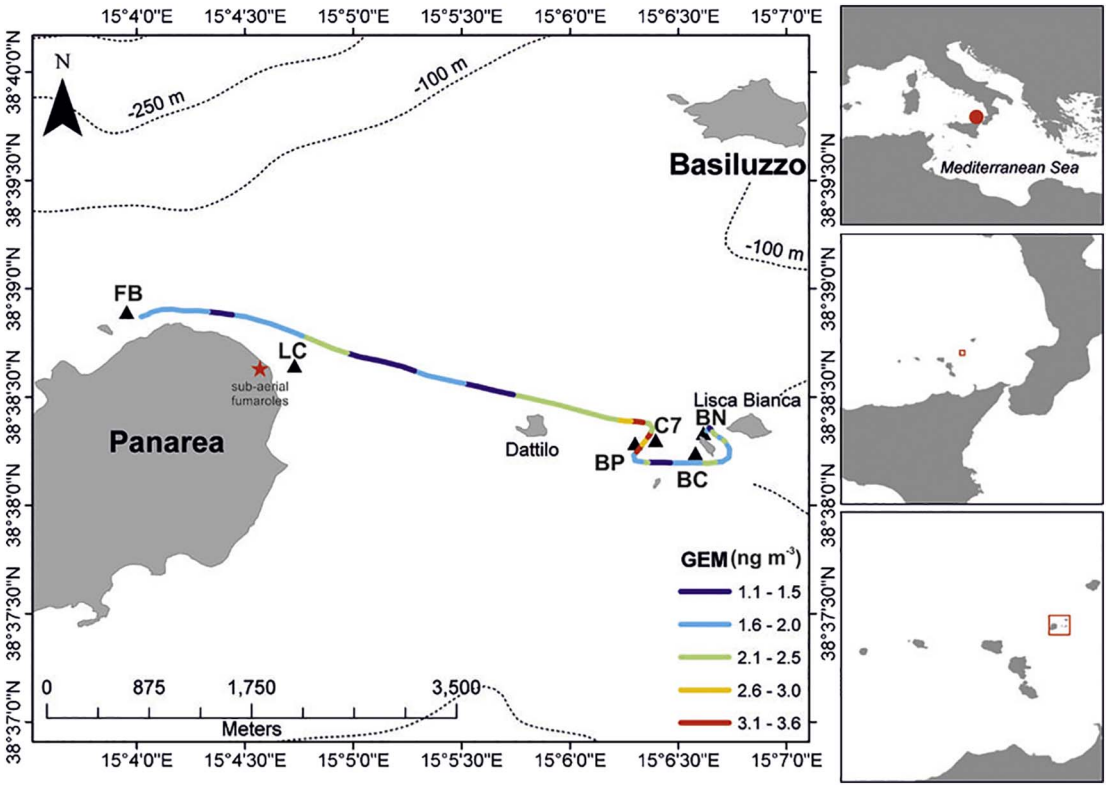

Fig. 3. Cruise tracks for atmospheric GEM distribution (at 3 m a.s.l) over the discharging area east of Panarea during the cruise campaign in November 2015. The degassing vent sites locations are also reported (black triangles) For the labels over each station, see caption of Fig. 1.

surface DGM concentrations through the enhancement of the release process (Wanninkhof, 1992) and is an important factor to consider when estimating the mercury emission rate from the sea surface.

Finally, we also quantified the GEM concentrations in the inland subaerial fumaroles located at the northeastern shoreline of the island (Fig. 1). Our intention was to distinguish the potential contribution from the inland degassing to the submarine hydrothermal Hg evasional flux in the marine boundary layer, at least during our survey. Fumaroles were collected by placing an inverted funnel (30 cm diameter) precisely on the gas vent to be sampled, which was connected to a glass condenser for the removal of the water vapor from the gas emission. This apparatus allowed us to convey gases directly into the Lumex mercury analyzer, which actively pumped them at 10 l min^{-1} with a sampling time of 1 s. Each acquisition lasted for about 5 min in a real-time continuous mode, until a stationary concentration data signal was achieved.

3. Results and discussion

3.1. Environmental parameters

The presence of hydrothermal leaks affected the chemistry of the seawater surrounding the vents. This was due to the increased levels of dissolved and free gas in the water, which modified some of the main parameters such as the pH and redox, with strong influences on the local environment. Scuba divers performed underwater vertical samplings, at different depths, to verify the real extent of such an effect. The pH was a very useful tracer of the dispersion of vent discharges, which revealed a direct relationship between proximity to the gas emission and increased acidification (Table 1): the lowest pH values were measured close to the sea floor, where the concentrated, acidic waters were constrained by their buoyancy (range: 6.08–7.83; Table 1). At the control site (FB), the pH value did not vary with depth and was always > 8, while the temperature showed a decreasing surface-bottom gradient from 20 to 14.7 °C. Conversely, the hydrothermal fluids exhibited very low pH values, ranging from 4.7 to 5.7. The redox values highlighted reducing conditions in both the hydrothermal fluids and the bottom waters close to the gas emissions (Eh values from − 235 to − 80 mV and from − 32 to 235 mV, respectively; Table 1). This was due to reduced sulphur (H_2S) in the gas seeping from the seafloor. Minor differences among the Eh values measured in the hydrothermal fluids indicated a dilution by seawater within the discharging vents during the rise towards the seafloor and/or within smaller shallower aquifers.

3.2. Geochemistry of the hydrothermal vents

Submarine vents were investigated by collecting samples of free gases and thermal waters from May to September 2015. The values were averaged to obtain a general picture composition of the fluids, as reported in Table 2. The data show the typical characteristics of the geothermal fluids, with the chemical and isotopic composition indicating the presence of a significant magmatic component. The sampled gases were mainly CO_2 (94–99 vol%), H_2S (0.2–6 vol%) and N_2 (0.2–2 vol%), with relatively low amounts of CH_4 (0.0001–0.4 vol%), H_2 (0.0001–0.07 vol%) and traces of CO (3×10^{-5}–3×10^{-4} vol%) (Table 2). This composition was the result of the interaction between original deep gases and seawater, at a relative low temperature (from 30 to 100 °C), at equilibrium with the atmosphere. The gas-seawater interaction causes both the condensation of steam and the loss of the highly soluble acid species (i.e., SO_2, HCl, HF) present in the original deep gases. There was a negative correlation (r^2 = 0.98) between the most abundant species in the gas phase of our samples, CO_2 and H_2S, indicating that the more CO_2 occurred in the dry gas phase, the less H_2S was detected (Fig. 4). The five investigated sites can be distinguished from each other using this ratio. The highest concentrations of CO_2 and the lowest concentrations of H_2S were determined for the BP and LC sites (Table 2). In contrast, the lowest CO_2/H_2S ratios were determined

Table 1
Chemical composition of the thermal and sea water samples in comparison with local seawater (Field Blank).

Location	Date	Longitude	Latitude	Sample type	Depth m	T °C	Eh mV	pH	Cond mS/cm	FTHg pM	RHg pM	DGM pM
Campo 7	6/15/2015	38° 38′ 16″ N	15° 06′ 24″ N	Surface water	5	21.2	139.4	8.08	58.5	8.39	7.28	n.d.
				Mid water	10	19.2	34.1	8.08	59.1	5.27	7.86	n.d.
				Bottom water	21.3	21.6	− 3.7	7.83	54.2	5.75	5.49	n.d.
				Thermal water	21.3	n.d.	− 193	4.76	57.1	3674.16	2.84	0.53
La Calcara	6/16/2015	38° 38′ 721 N	015° 09′ 646 N	Surface water	5	20.8	− 31	8.13	56.8	7.88	3.56	0.1
				Mid water	10	18.9	− 51.1	8.16	57.7	5.77	1.80	n.d.
				Bottom water	19	17.9	− 20.8	7.9	58	5.33	3.54	n.d.
				Thermal water	19	n.d.	− 80	5.09	50.7	2432.82	6.18	5.6
Bottaro Crater	6/17/2015	38° 38′ 233 N	015° 06′ 577 N	Surface water	5	22.6	− 15.2	8.08	55.6	3.98	4.37	0.09
				Bottom water	12.4	21.5	− 55	7.82	56.5	5.40	4.91	n.d.
				Thermal water	12.4	n.d.	− 182.4	5.55	59	1071.84	7.85	1.58
Bottaro North	6/17/2015	38° 38′ 20″ N	15° 06′ 37″ E	Surface water	2	21.4	− 132.5	7.35	54.8	3.38	4.87	0.05
				Bottom water	7.7	22.6	− 167.3	6.08	55.8	5.27	4.78	n.d.
	6/18/2015			Thermal water	7.7	n.d.	− 235	5.71	56.9	1824.62	4.60	0.27
Black Point	6/17/2015	38° 38′ 13″ N	15°06′ 18″ E	Surface water	5	18.3	139.9	8.16	56.3	5.92	5.08	0.22
				Mid water	10	18.7	111.8	8.18	56	6.31	6.29	n.d.
				Bottom water	22.9	17.4	− 42.4	7.11	55.4	7.05	5.28	n.d.
	6/18/2015			Thermal water	22.9	n.d.	− 87	5.58	56.3	4711.10	4.60	0.24
Field Blank	6/17/2015	38° 38′ 892 N	015° 01′ 954 E	Surface water	5	20.3	24.2	8.05	55.2	4.20	7.19	0.01
				Mid water	10	20.2	11.6	8.11	55.2	5.13	5.93	n.d.
				Bottom water	25	14.7	7.5	8.15	55.9	3.88	5.29	n.d.

n.d. = not determined

at the BN vent site, while the gases sampled at BC and C7 showed ratios between both clusters (Table 2 and Fig. 4). The different CO_2/H_2S ratio among the sites indicates the occurrence of gas scrubbing, whereas the extent of partial gas dissolution with respect to the different solubility in seawater may be an indicator of the velocity of the gas ascent towards the seafloor. Accordingly, the gases of large fumaroles which are probably characterized by rapid gas migration, suffered the least dissolution of the more soluble H_2S, which explains the lowest CO_2/H_2S ratio analyzed in these gas samples. This is particularly conceivable for BN (Table 2), which is the strongest and shallowest site of the studied vent areas and the only one where the gas plumes reached the surface, creating a "blowout" surrounded by pseudo-convective cells (Fig. 5). This effect can strongly influence the mixing between the inner water that is more affected by the presence of CO_2 and the surrounding water.

The helium isotopic ratio measured in the fluids, normalized to the atmosphere ($^3He/^4He_{atm} = 1.39 \times 10^{-6}$) and expressed as R/R_{air} was about 4.3 ± 0.2, indicating that the hydrothermal reservoir feeding the submarine hydrothermal field was affected by the significant contribution of fluids released from a magmatic body. Furthermore, the $^4He/^{20}Ne$ isotopic ratios are up to three orders of magnitude higher than the atmosphere, ranging from 67 to 210 (Table 2).

Chemical analyses of the discharged thermal waters showed that all the samples had a seawater-like Na-Cl composition (Table 3; Fig. 6a), with the specific on-site parameters revealing the occurrence of mixing between ambient seawater and a thermal end-member, according to previous investigations (Tassi et al., 2009; Gugliandolo et al., 2006; Italiano and Nuccio, 1991; Caliro et al., 2004). Given the calculated equilibrium temperatures, the recorded thermal water compositions confirmed that there are high temperature water-rock interactions inside the deep geothermal body, as proposed by Tassi et al. (2009). The

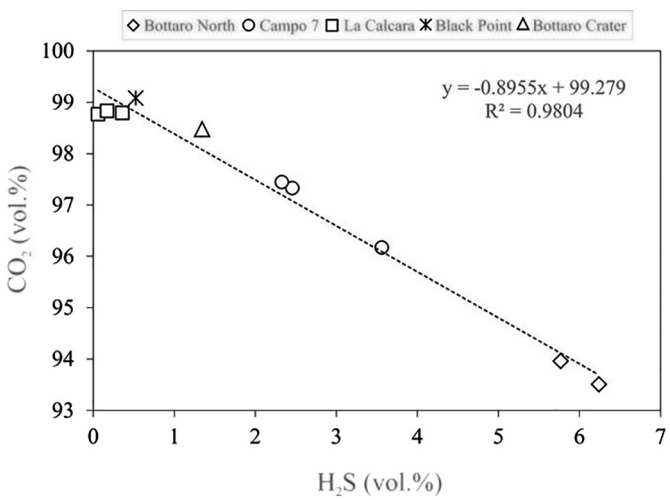

Fig. 4. Correlation between CO_2 and H_2S in the collected gas phase of hydrothermal fluids ($r^2 = 0.98$). The negative correlation indicates that the more CO_2 occurred in the dry gas phase, the less H_2S is detected.

chemical composition of the BP and LC samples showed a slight depletion in Na^+ and Mg^{2+} compared to the seawater, whereas K^+ and Ca^{2+} were more concentrated (Table 3). Several authors have demonstrated that Mg can be easily removed from seawater heated by an interaction with hot rocks and hydrothermal fluids through the precipitation of clays such as Mg-rich smectite and chlorite (Tivey, 2007). Among the major water components, SO_4^{2-} was the only one who showed a positive correlation with Mg ($r^2 = 0.84$; Fig. 6b), suggesting

Table 2
Mean chemical composition (in vol%) of the gases sampled during May–September 2015. The CO_2/H2S molar ratios measured in the fluids are reported, together with the $^4He/^{20}Ne$ isotopic ratios and the helium isotopic ratios normalized to the atmosphere (R/Rair). Gaseous elemental mercury concentrations Hg^0 (in ng/m^3) are also reported.

Location	He	H_2	N_2	CO	CH_4	CO_2	H_2S	O_2	CO_2/H_2S	Hg^0	$^4He/^{20}Ne$	R/R_{air}
Bottaro North	0.0012	0.0004	0.26	5.1E − 05	0.0001	93.7	6.0	0.04	15.6	7600	136.2	4.3
Campo 7	0.0007	0.0001	0.22	3.1E − 05	0.017	97.0	2.8	0.05	34.8	1893.3	210.8	4.2
La Calcara	0.0004	0.0721	0.49	1.2E − 04	0.443	98.8	0.2	0.1	499.8	3500	67.4	4.3
Black Point	0.001	0.0124	2.00	3.1E − 04	0.079	97.2	0.7	0.03	144.3	624.4	188.9	4.3
Bottaro Crater	0.001	n.d.	0.18	1.1E − 04	0.002	98.5	1.3	0.2	73.3	6400	138.3	4.2

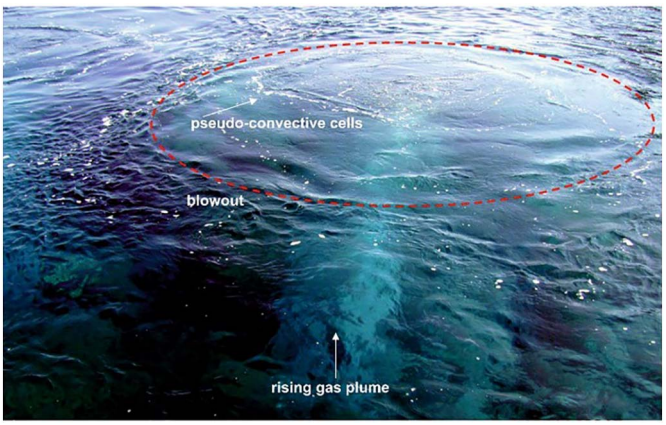

Fig. 5. Sea-surface manifestation of the "blowout" surrounded by pseudo-convective cells created by the rising submarine gas plume from the Bottaro North discharging vent.

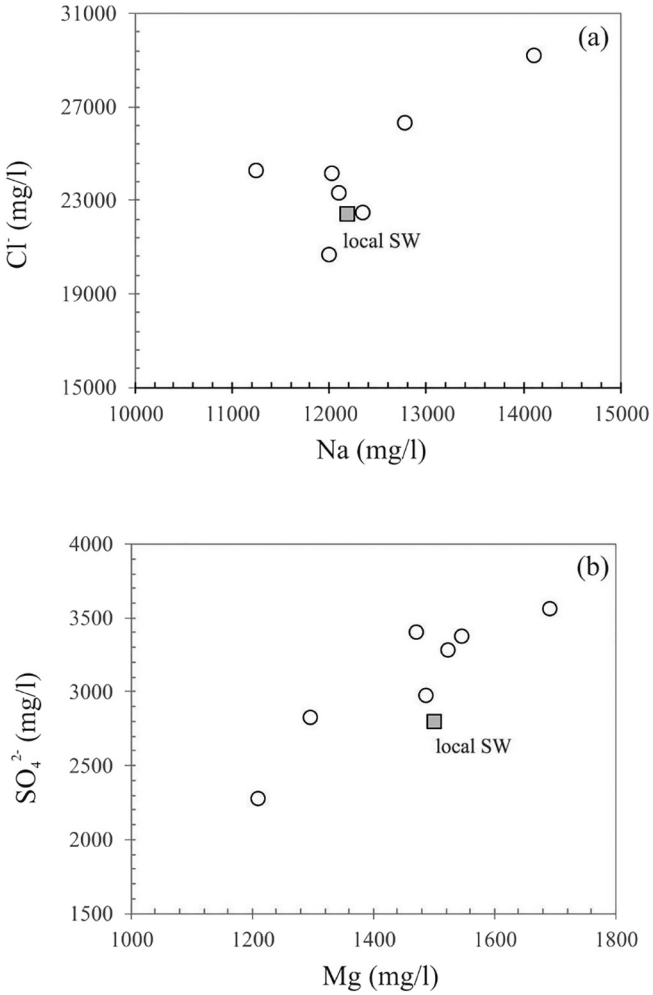

Fig. 6. (a) Na vs. Cl^- and (b) Mg vs. SO_4 binary diagrams for the thermal water samples from the submarine fumarolic field of Panarea Island.

that like Mg, SO_4^{2-} is strongly depleted in the deep end-member (Tassi et al., 2009). Conversely, the higher Mg and SO_4^{2-} concentrations found in the lasting samples may be viewed as resembling those of "concentrated seawater", that is seawater affected by boiling due to heat rising from the deep system that significantly increases salinity (Tassi et al., 2009).

3.3. Hydrochemical mercury distribution

3.3.1. FTHg and RHg distribution in the seawater column

We investigated the vertical distribution of the FTHg and RHg in the seawater column overlying the selected vents in order to examine the influence of mercury vented from the submarine fumaroles in the surrounding marine environment. The mean concentration of FTHg in the surface water was 5.9 ± 2.2 pM, with a range from 3.3 to 7.8 pM (Table 1). These data were slightly higher than that reported for open seas, such as the Pacific Ocean (1.15 ± 0.86 pM; Laurier et al., 2004) and the Atlantic Ocean (from 2.4 ± 0.6 to 2.9 ± 1.2 pM; Mason et al., 1998; Mason and Sullivan, 1999). They were, however, comparable to values reported in some near-shore environments, such as the Black Sea (1.6–10.4 pM; Lamborg et al., 2008) and the coastal site of the Yellow Sea (13.3 pM; Ci et al., 2011). Conversely, our data resulted somewhat higher than previous records in the literature for the Mediterranean Sea (1.46 ± 0.41 pM, Horvat et al., 2003; 1.32 ± 0.48 pM, Kotnik et al., 2007, 2013; 2.54 ± 1.25 pM, Cossa et al., 1997), emphasizing the importance of considering submarine hydrothermal activity as an additional potential source of Hg for the Mediterranean area. On the whole, the spatial distribution of FTHg with depth showed no significant variations, although the bottom waters just above the BC, BN and BP vents were characterized by weak Hg enrichments (Table 1). Probably, in this highly energetic environment the presence of efficient currents produces vertically mix and uniform the water column. Furthermore, the formation of pseudo-convective cells (Fig. 5), and the related current triggered by the water movement, may act as a sort of "liquid barrier" that reduces the direct contact between the inner plume and the surrounding seawater (McDougall, 1978). Therefore, the mixing between the more Hg-rich water inside the plume and the surrounding seawater environment was reduced. In fact, the FTHg concentrations measured in the near-bottom seawaters of the hydrothermal vents ranged from 5.2 to 7 pM, with a mean value of 5.76 ± 0.7 pM (Table 1). The average RHg concentration in the surface waters was 5.03 ± 1.39 pM, with a range of 3.5–7.3 pM, accounting for the dominant fraction of FTHg (%RHg/FTHg = 85%; Fig. 7). These RHg values were generally higher than those proposed for many other open oceans elsewhere (Atlantic Ocean: 0.8 ± 0.44 pM, Mason and Sullivan, 1999; Pacific Ocean: 0.47–1.85 pM; Mason and Fitzgerald, 1990, 1993; Antarctic Ocean: 0.6–1.25, Dalziel, 1995). They were also higher than the records recently attained for the Mediterranean Sea, as well (0.38 ± 0.29 pM, Kotnik et al., 2007, 2013; 0.02–0.97 pM, Cossa et al., 1997; 0.81 ± 0.32 pM, Horvat et al., 2003). The spatial distribution of RHg with depth showed no important variations, with the

Table 3
Chemical composition of the submarine thermal waters discharged at Panarea Island. The measured chemical composition of local seawater SW (collected at the Field Blank site in June 2015) is also reported. Ion contents are in mg/l.

Location	Depth	pH	HCO_3^-	Cl^-	SO_4^{2-}	Na	K	Ca	Mg
Campo 7	21.3	4.76	207	26,345	3376	12,784	511	30	1546
La Calcara	19	5.09	268	24,285	2829	11,239	493	796	1296
Bottaro Crater	12.4	5.55	146	29,200	3567	14,112	536	559	1691
Bottaro North	7.7	5.71	128	20,684	2972	11,991	447	454	1486
Black Point	22.9	5.58	55	24,158	2274	12,025	868	1815	1210
local SW	25	8.15	153	22,405	2804	12,180	465	474	1499

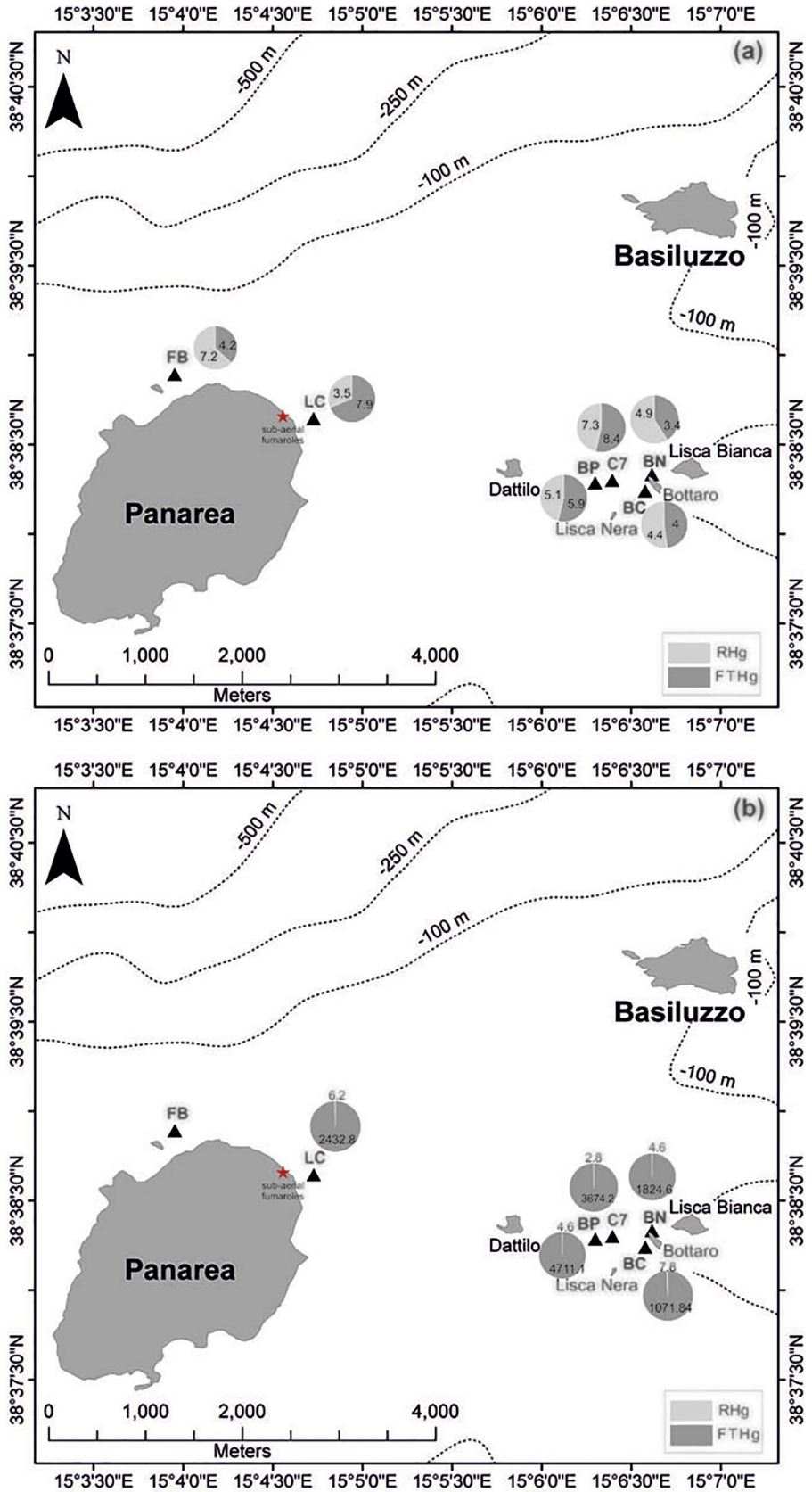

Fig. 7. Spatial distribution of the total filtered Hg (FTHg, unit in pM) and reactive Hg (RHg, unit in pM) in (a) the surface sea-waters and (b) hydrothermal fluids, respectively.

concentrations measured in the bottom seawaters ranging from 3.5 to 5.5 pM (mean: 4.8 ± 0.7 pM; Table 1). Minor discrepancies in the FTHg and RHg distributions observed between the surface and the bottom seawater may be the result of sunlight, temperature and other physical-chemical parameters that strongly affect mercury speciation at shallower depths. RHg in aquatic environments is generally considered

to be the available fraction of Hg for biogeochemical processes such as the reduction to Hg^0 and the conversion to mono-methylmercury (Morel et al., 1998; Amyot et al., 1997). Accordingly, the measured high RHg and RHg/FTHg ratios suggest that the turnover time of Hg in the investigated waters may be shorter than the other marine systems. Similar data have been obtained for seawater collected close to the gas seeping site of a submarine geothermal field in Kagoshima Bay (FTHg: 0.25–15 pM and RHg: 0.03–7.33 pM; Tomiyasu et al., 2007), where as much as 200 mg kg^{-1} of Hg was measured in the sediment near the fumaroles (Sakamoto, 1985).

3.3.2. FTHg and RHg in the hydrothermal waters

The measured FTHg concentrations in the hydrothermal fluids ranged from 1072 to 4711 pM (mean: 2743 ± 1455 pM), with the highest values found in the fluids collected at the BP and C7 stations (Table 1). In general, the FTHg in these fluids was up to three orders of magnitude higher than in the ambient seawater (FB) (Table 1), demonstrating that the control area was unaffected by the submarine hydrothermal activity. The FTHg contents in the hydrothermal fluids showed a clear difference from the water column over the vent, due to efficient dilution. Compared with other studies, our FTHg concentrations were somewhat higher than those identified in the thermal waters collected at the Sea Cliff submarine hydrothermal field in the North-East Pacific Ocean (4–10 pM; Lamborg et al., 2006). They were, however, well below the values observed in the submarine hot fluids collected at Bahía Concepción (FTHg ~10^6 pM; Prol-Ledesma et al., 2004), which is one of the largest fault-bound bays in Baja California, Mexico.

Simultaneous measurements of RHg in the hydrothermal fluids gave values in the range of 2.84–6.85 pM (mean: 5.21 ± 1.9 pM), accounting for a very low portion of FTHg (%RHg/FTHg = 0.1–0.7%) (Table 1 and Fig. 7), but these were higher than the values reported for many other open oceans elsewhere (Table 4). The trivial RHg/FTHg ratio may indicate that, in submarine hydrothermal fields, significant fractions of RHg are probably involved in reducing the biotic (that is enzymatically catalyzed by microorganisms) and abiotic mechanisms that turn Hg^{2+} into DGM form (Ferrara et al., 2003; Mason et al., 1995; Ci et al., 2011; Dekov, 2007; Fitzgerald et al., 2007; Rolfhus and Fitzgerald, 2004; Poulain et al., 2007; Fantozzi et al., 2009). These processes may significantly contribute to the supersaturation of DGM found in seawater and to the emission of Hg^0 into the atmosphere.

3.3.3. DGM concentrations

DGM consists of elemental and dimethyl Hg (Hg^0 and $(CH_3)_2Hg$, respectively). In this study, we assume that DGM overall occurs as dissolved elemental mercury (DEM or Hg^0) since, in the upper ocean, Hg^0 is the dominant form of DGM (~90%, Gardfeldt et al., 2003; Laurier et al., 2004). Meanwhile, detectable MMHg was only documented in deep seawater (Amyot et al., 1997; Mason et al., 1995). The DGM in water can be transported via currents, reacting chemically or biologically, or may ultimately be released into the atmosphere. The highest DGM concentrations were detected in the hydrothermal fluids (Fig. 8a), within a range of 0.2–5.6 pM (Table 1), accounting for a small fraction of the FTHg (0.01–0.2%) and representing from 5 to 90% (average 28%) of the inorganic RHg. These results suggest that while DGM is produced in surface water mainly as a consequence of photo-induced reactions (Amyot et al., 1997; Fantozzi et al., 2007, 2009; Lanzillotta and Ferrara, 2001; Lanzillotta et al., 2002; Qureshi et al., 2010), photochemical reduction may be excluded as a possible means of Hg^0 formation in the deeper thermal waters. Meanwhile, the deep water hydrothermal and/or bacterial activities may constitute an additional significant source of DGM (Amyot et al., 1997; Costa and Liss, 1999, 2000; Gårdfeldt et al., 2001; Lanzillotta and Ferrara, 2001; Lanzillotta et al., 2002; Ferrara et al., 2003; Gustin et al., 1999; Horvat et al., 2003; Kotnik et al., 2007, 2013). To date, however, we cannot distinguish mercury contributions provided by the bacterial activity in the sediment from those derived from the hydrothermal activity. It seems probable, however, that they both contributed to the higher values of the DGM concentrations observed in the collected deep thermal fluids of Panarea.

In shallow seawater (~5 mt), we measured DGM concentrations varying from 0.05 to 0.22 pM (average: 0.12 ± 0.07 pM; Fig. 8b and Table 1), which accounted for about 2% of both the FTHg and RHg. Unlike the LC and BC stations, which had the highest DGM values in the hydrothermal fluids (5.6 and 1.6 pM, respectively), in general, our current estimates are comparable to the DGM presented by previous authors for the Mediterranean area (0.08–0.4 pM; Cossa et al., 1997; Ferrara et al., 2003; Cossa and Coquery, 2005; Horvat et al., 2003; Fantozzi et al., 2013; Table 5). Similar values are also reported for some polluted marine areas, such as Tokyo Bay (0.18–0.34 pM; Narukawa et al., 2006), the Yellow Sea (0.4–0.25 pM; Ci et al., 2011), the South China Sea (0.26–0.11 pM; Fu et al., 2010), and most coastal regions elsewhere, such as Long Island Sound (0.07–0.33 pM; Rolfhus and Fitzgerald, 2001), Chesapeake Bay (0.12–0.25 pM; Mason and Sullivan, 1999), the Baltic Sea (0.09 pM; Wangberg et al., 2001), and the Ionian Sea (0.1–0.25 pM; Andersson et al., 2007). These data are comparable to those reported for the North and Equatorial Atlantic Ocean (0.48 ± 0.31 and 1.2 ± 0.8 pM, respectively; Mason et al., 1998; Mason and Sullivan, 1999) and the Equatorial Pacific (0.04–0.32 pM; Mason and Fitzgerald, 1990, 1993) (Table 5). Certainly, minor differences in DGM concentrations between the marine areas cited above may be explained by the different biogeochemical, hydrodynamic and geotectonic scenarios.

3.3.4. Elemental gaseous mercury in deep-rising bubbles

Mercury may be partially released from hydrothermal vents as a

Table 4
Literature data on FHg and RHg measured in both hydrothermal fluids and seawater reported elsewhere; n.a. = not available data.

Location	Sample type	FTHg pM	RHg pM	References
Pacific Ocean	Surface seawater	1.15 ± 0.86	0.47–1.85	Laurier et al., 2004; Mason and Fitzgerald, 1990, 1993
Atlantic Ocean	Surface seawater	2.4 ± 0.6 to 2.9 ± 1.2	0.8 ± 0.44	Mason et al., 1998; Mason and Sullivan, 1999
Mediterranean Sea	Surface seawater	1.32 ± 0.48 to 2.54 ± 1.25	0.02 to 0.97	Horvat et al., 2003; Kotnik et al., 2007; Cossa et al., 1997
Black Sea	Surface seawater	1.6 to10.4	n.a.	Lamborg et al., 2008
Yellow Sea	Surface seawater	13.3	n.a.	Ci et al., 2011
Antarctic Ocean	Surface seawater	n.a.	0.6 to 1.25	Dalziel, 1995
Kagoshima Bay	Bottom seawater	0.25 to 15	0.03 to 7.33	Tomiyasu et al., 2007
Mid-Atlantic Ridge	Bottom seawater	0.07–1.10 × 10^{-3}	n.a.	Carr et al., 1975
Sea Cliff, North-East Pacific	Thermal water	4 to 10	n.a.	Lamborg et al., 2006
Bahía Concepción	Thermal water	1,000,000	n.a.	Prol-Ledesma et al., 2004
Panarea, South Tyrrhenian Sea	Surface seawater	3.3 to 7.8	3.5 to 7.3	This study
Panarea, South Tyrrhenian Sea	Bottom seawater	5.2 to 7	3.5 to 5.5	This study
Panarea, South Tyrrhenian Sea	Thermal water	1072 to 4711	2.84 to 6.85	This study

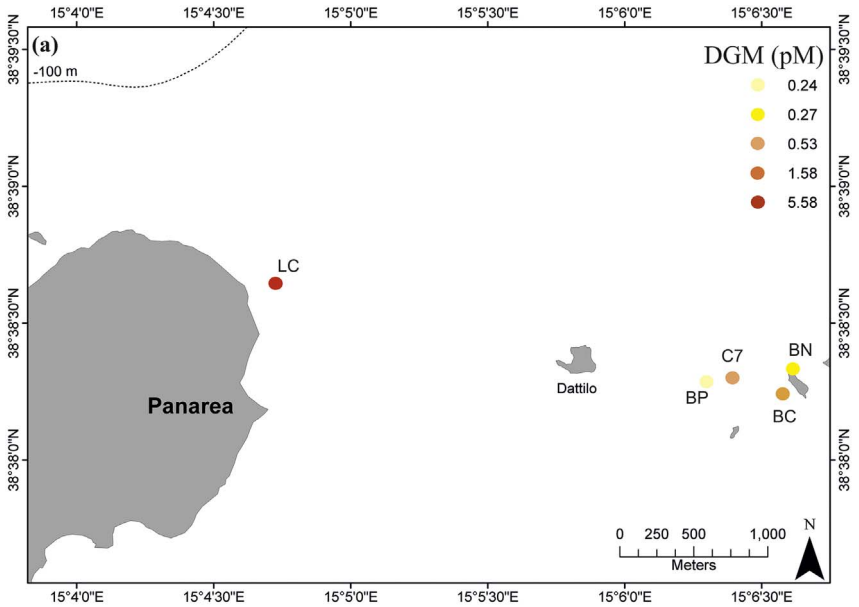

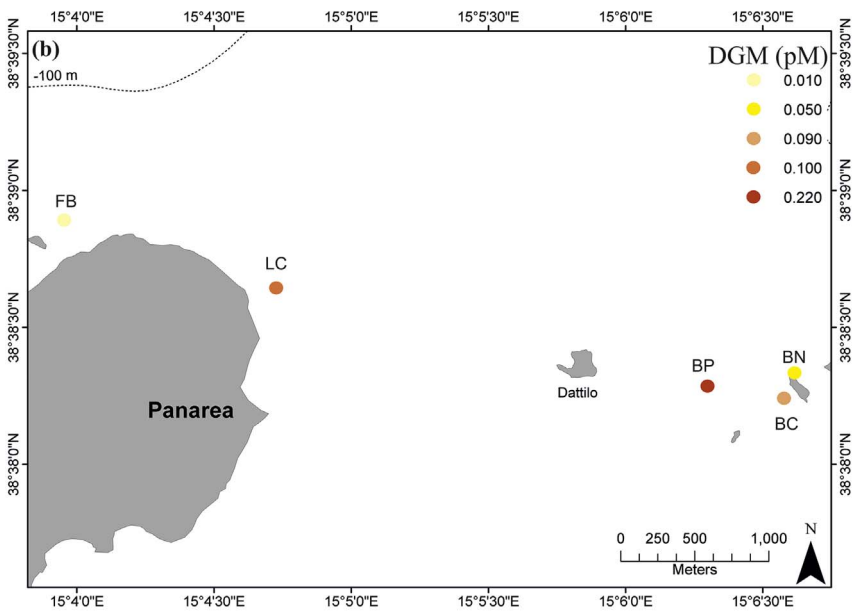

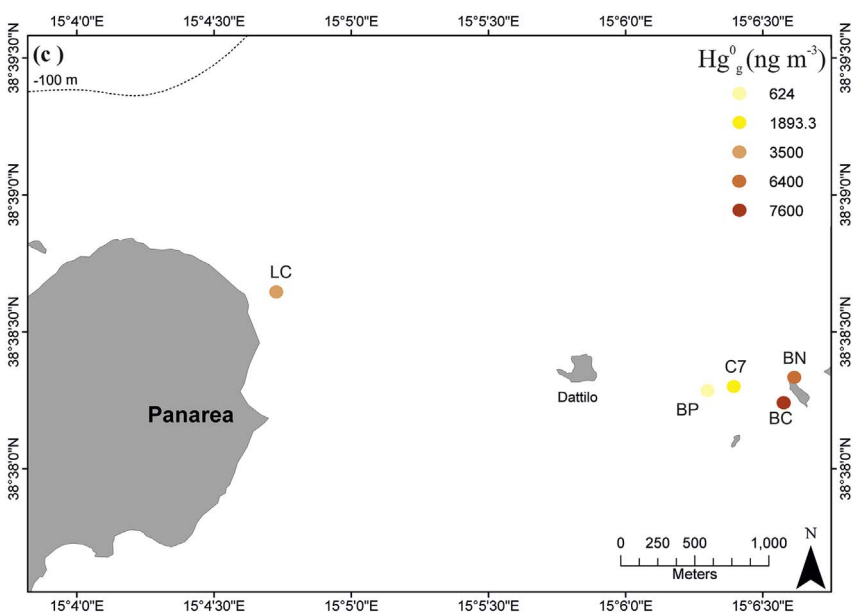

(caption on next page)

Fig. 8. Spatial distribution of DGM concentrations in the (a) surface waters and (b) hydrothermal fluids, respectively along the route followed by the RV *Bio4You* during the cruise campaigns (June and November 2015). (c) Elemental mercury concentrations (Hg^0_g) in the hydrothermal dry gas phase of the collected thermal waters are also reported. Labels indicate: LC, La Calcara; BP, Black Point; BN, Bottaro North; BC, Bottaro Crater, C7, Campo 7; FB, Field Blank.

Table 5
Dissolved gaseous mercury (DGM) concentrations (in pM) for different water bodies worldwide.

Location	DGM	References
East Mediterranean	0.37	Kotnik et al., 2007
East Mediterranean	0.13	Kotnik et al., 2007
East Mediterranean	0.08	Fantozzi et al., 2013
East Mediterranean	0.2	Fantozzi et al., 2013
East Mediterranean	0.2	Gardfeldt et al. 2003
Western Mediterranean	0.32	Cossa et al., 1997
Western Mediterranean	0.39	Cossa et al., 1997
Tyrrhenian Sea	0.1	Gardfeldt et al., 2003
Strait of Sicily	0.43	Gardfeldt et al., 2003
Atlantic coastal water	0.11	Gardfeldt et al., 2003
Ionian Sea	0.18	Andersson et al., 2007
Ionian Sea	0.25	Andersson et al., 2007
Ionian Sea	0.08	Andersson et al., 2007
Ionian Sea	0.14	Andersson et al., 2007
Baltic Sea	0.09	Wangberg et al., 2001
Tokyo Bay	0.18	Narukawa et al., 2006
Tokyo Bay	0.34	Narukawa et al., 2006
Long Island Sound	0.07	Rolfhus and Fitzgerald, 2001
Long Island Sound	0.33	Rolfhus and Fitzgerald, 2001
Chesapeake Bay	0.12	Mason and Sullivan, 1999
Chesapeake Bay	0.25	Mason and Sullivan, 1999
Yellow Sea	0.39	Ci et al., 2011
Yellow Sea	0.25	Ci et al., 2011
Chesapeake Bay	0.12	Mason and Sullivan, 1999
Chesapeake Bay	0.25	Mason and Sullivan, 1999
South China Sea	0.26	Fu et al. 2010
South China Sea	0.11	Fu et al. 2010
Rosignano Solvay coastal water	0.15	Ferrara et al., 2001
Rosignano Solvay coastal water	0.65	Ferrara et al., 2001
Rosignano Solvay coastal water	0.25	Fantozzi et al. 2007
Rosignano Solvay coastal water	0.46	Fantozzi et al. 2007

component of hydrothermal gas bubbles (Hg^0_g), rising through the water column up to the marine surface. There is a lot of interest in the role of the bubbling process at the ocean's surface on gas supersaturation. To date, data are mainly provided from studies of gas transfer and the interpretation of highly insoluble trace gas concentrations (Craig and Weiss, 1971; Fuchs et al., 1987), but there is still too much of a gap in the knowledge to formulate a satisfactory theory. Recent studies have, however, shown that bubbles play an important role in the ocean-atmosphere exchange of gases on the sea surface, providing an additional air-water interface for the transfer of gases and speeding up the rate of equilibration (Zhang, 2012; Hamme and Emerson, 2002, 2006; D'Asaro and McNeil, 2007; Vagle et al., 2010).

At Panarea, as a bubble rises, more soluble hydrothermal gases such as CO_2 will rapidly dissolve in the water column in the initial few meters (Langmuir, 1977). Meanwhile, while Hg^0_g will mainly transfer up to the surface and escape into the atmosphere, due to its high volatility (Henry coefficient < 0.3; Mason et al., 1994) and low solubility in water (60 μg/l at 25 °C; Sarkar, 2003). The Hg^0_g concentrations in the dry gas phase (i.e. bubbles) of the thermal waters were in the range 624–7600 ng m^{-3} ($\sim 7.6 \times 10^{-5}$–9.3×10^{-4} ppm; Table 2), with the highest values measured in the samples collected at the shallowest submarine vents, such as BN and BC (at depths of 7.7 and 12.4 m, respectively). These data confirm that the solubility of Hg^0_g vapor in seawater at about 20–30 °C obeys Henrys Law (Fig. 9). The negative correlation between the DGM and vapor Hg^0_g concentrations found in the collected fluids is then justified, suggesting that, at the same hydrostatic pressure (or related depth), less Hg^0_g is detected when there is more DGM in the deeper hydrothermal fluids. Unfortunately, since the

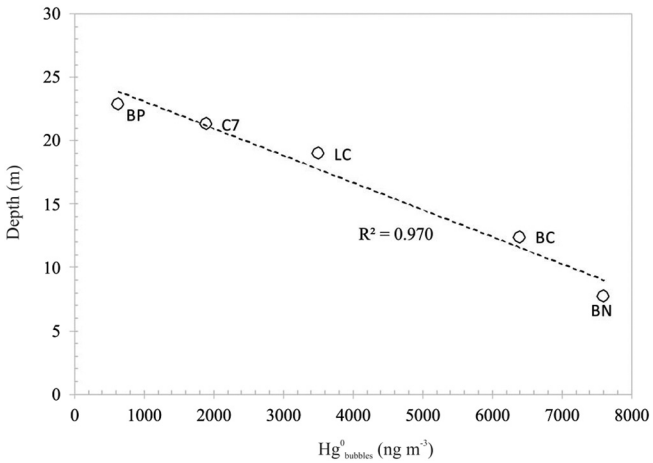

Fig. 9. DGM and Hg^0 (bubbles) concentrations vs. depth in the collected hydrothermal fluids of Panarea Island. BN: Bottaro North; BC: Bottaro Crater; LC: La Calcara; FB: Field Blank.

Hg^0_g concentrations in the dry gas phase vented from submarine hydrothermal activity have not been measured to date, a comparison with other studies is not currently possible.

3.4. Atmochemical mercury distribution

3.4.1. GEM dispersion in the marine boundary layer over the hydrothermal vents

The cruise track and the GEM concentrations measured at 3 m above sea level are shown in Fig. 3. The overall average concentration was 1.9 ± 0.6 ng m^{-3}, with a range from 1.1 to 3.6 ng m^{-3}. Additional atmospheric GEM acquisitions were also performed at ~1.5–2 m above sea level and from the stationary vessel, with the aim being to reduce air turbulence and dilution. These additional measurements provided higher atmospheric GEM concentrations over each site (range: 1.8 ± 0.5–6.4 ± 2.6 ng GEM m^{-3}; Table 6), with the maximum GEM value measured over the intensive exhaling vents at the BN station, characterized by a strong volcanic gas bubbling that was clearly visible at the sea surface (Fig. 5). In addition, the smell of hydrogen sulphur (H_2S) was significant during the sampling, confirming the rise of gas bubbles that transport Hg^0_g from the seafloor to the shallow levels. High atmospheric GEM concentrations were also measured at the BP station (4.82 ± 1.36 ng m^{-3}), while intermediate values were detected in the remaining investigated vent sites (Table 6). These data were higher than the values measured in the marine boundary layer over the selected Panarea control site (FB, 1.7 ± 0.35 ng GEM m^{-3}). More generally, they were also higher than the background GEM levels reported for the northern hemisphere (1.58 ± 0.04 ng m^{-3}, Steffen et al., 2005), as well as other marine areas elsewhere (Equatorial Pacific Ocean, 1.0 ± 0.1 ng m^{-3}, Kim and Fitzgerald, 1986; North Atlantic Ocean, 2.1 ± 0.8 ng m^{-3}, Mason et al., 1998; Baltic Sea, 1.6 ± 0.2 ng m^{-3}, Wangberg et al., 2001). Recent investigations performed in the Mediterranean Basin, gave atmospheric GEM values lower than those reported in this study (range: 1.73–1.8 ng m^{-3}; Gardfeldt et al., 2003; Kotnik et al., 2013). Finally, our new data were clearly higher than the atmospheric GEM concentrations measured in the MBL overlying the submarine hydrothermal vents of the Piip Volcano, in the Bering Sea (0.8–2 ng m^{-3}, Astakhov et al., 2011).

Table 6
Summary of station information, atmospheric GEM, surface water DGM and relevant data for air-sea Hg (0) flux calculation in the hydrothermal area east of Panarea Island during the cruise in November 2015. K_w values resulted by using both Wanninkhof (1992) (W92) and Nightingale et al. (2000) (N2000) parametrization have been reported for comparison, and the relative air-sea Hg0 flux estimates as well.

Location	GEM ng m^{-3}	DGM pg l^{-1}	S_a	K_w (N2000) m h^{-1}	K_w (W92) m h^{-1}	u_{10} m s^{-1}	Hg^0 Flux (N2000) ng m^{-2} h^{-1}	Hg^0 Flux (W92) ng m^{-2} h^{-1}
Black Point	4.8	44.4	2.6	0.061	0.065	4.6	8.7	9.1
La Calcara	2.9	20.5	1.9	0.067	0.071	4.8	4.2	4.5
Bottaro Crater	1.8	18.7	2.8	0.056	0.058	4.4	3.4	3.5
Bottaro North	6.4	9.5	0.4	0.061	0.065	4.6	0.7	0.7

3.4.2. GEM in the inland subaerial fumaroles

Inland GEM determinations in the sub-aerial fumarolic emissions were performed during the first geochemical survey on 17th June 2015. We aimed to evaluate the potential contribution of the natural lands degassing to the estimated hydrothermal Hg flux at the sea-air interface. During the sampling, the fumarolic emissions had a temperature of ~100 °C, while air temperature and wind velocity were 29 °C and 3 m s^{-1}, respectively. An inverted funnel connected to the mercury analyzer was used to capture gases, which were directly analyzed in the standard monitoring mode. We measured a mean (± SD) GEM concentration of 2652 ± 503 ng m^{-3}, with a range of 2099 to 3081 ng m^{-3}. These values differ a lot from those found in the diluted atmospheric marine boundary layer over the investigated vents (Table 6), suggesting that the contribution of the atmospheric land's outgassing does not impact the calculated marine Hg evasion flux.

3.5. Model for estimating Hg^0 flux

3.5.1. Degree of DGM saturation (S_a)

The combination of photo-physical processes and intense hydrothermal activity leads to naturally occurring, supersaturated DGM concentrations throughout the submarine degassing field east of Panarea Island and enhances the mercury evasion at the water-atmosphere interface. Assuming that all the DGM is dissolved elemental mercury (DEM or Hg^0), the saturation S_a is an indicator of Hg^0 emission and can be obtained from the following equation:

$$S_a = \frac{H' \times C_w}{C_a} \quad (1)$$

where C_w and C_a are the DGM concentrations in the seawater (pg l^{-1}) and the GEM concentrations in the atmosphere (ng m^{-3}), respectively. H′ is the dimensionless partitioning coefficient for Hg^0 between water and air (Henrys Law constant) calculated for seawater and corrected for temperature according to Andersson et al. (2008) and Sanemasa (1975). The S_a value > 1 indicates the supersaturation of Hg^0 in the surface water with respect to the Hg^0 in the air and the subsequent Hg^0 emission from the sea surface; otherwise, under-saturation is indicated and Hg^0 deposition from the atmosphere to the sea surface occurs.

Paired atmospheric GEM and DGM samples from our survey showed that most of the collected surface water was supersaturated with elemental mercury (Table 6). Similar scenarios have also observed elsewhere in the Mediterranean Basin, and documented by many authors (Horvat et al., 2003; Amyot et al., 1997; Fantozzi et al., 2007, 2009, 2013; Lanzillotta and Ferrara, 2001; Lanzillotta et al., 2002).

At Panarea, the degree of DGM supersaturation (S_a) was, on average, 2.5 ± 0.4, with a range of 1.9–2.8, leading to a net emission of Hg^0 from the sea surface into the atmosphere (Table 6). The relative variations in the saturation degree may, however, govern the flux. At the BN site, for example, where S_a < 1, the high atmospheric GEM value (Table 6) and the lowest DGM concentrations in the surface water, indicate that most of the gaseous Hg^0 contributions to the atmosphere are mainly due to the rise of gas bubbles to the surface that are enhanced by low hydrostatic pressure (i.e. low depth). Conversely, the control site (FB) usually produced an under saturation of DGM (S_a < 1), with low values of both DGM and GEM, confirming that this area was unaffected by submarine hydrothermal activity and promoting a potential net Hg^0 deposition from the atmosphere to the sea surface. Compared to other marine areas, our S_a values were lower than those reported in the literature for two polluted coastal areas, such as the Yellow Sea (7.8 ± 2.3; Ci et al., 2011) and Tokyo Bay (~10; Narukawa et al., 2006).

3.5.2. Air-sea exchange flux of Hg^0

The supersaturation of Hg^0 in the surface waters indicates that the exchange of Hg^0 would always be from the sea surface into the atmosphere at a rate dependent on: 1) the concentration of volatile forms of mercury in water and air, and 2) the water temperature and the wind speed (Liss, 1983; Wanninkhof, 1992). Studies of mercury evasion from seawater have been published in Europe and North America (Cossa et al., 1997; Rolfhus and Fitzgerald, 2001; Wangberg et al., 2001; Gårdfeldt et al., 2001, 2003), although mercury evasion from seawater due to an extreme submarine hydrothermal impact, as reported in this study, has not been observed to date.

To assess the potential mobilization of mercury through the air-sea gas exchange, we calculated the evasional Hg^0 flux from the data on DGM and other factors using the two-layer gas exchange model developed by Liss and Slater (1974). This assumes that the net exchange of a non-reactive gas depends on the molecular diffusion on either side at the air-sea interface. This model is based on the transfer coefficient and the Hg^0 gradient between the vapor phase (GEM in the atmosphere) and dissolved phases (DGM in the seawater), and it can be expressed as in Eq. (2):

$$F = K_w \cdot \frac{C_w - C_a}{H'} \quad (2)$$

where F is the estimated Hg^0 flux (ng m^{-2} h^{-1}) and K_w is the gas exchange velocity (cm h^{-1}), which primarily depends on the wind speed on the sea surface and the Schmidt number representing material transfer in a fluid (Wanninkhof, 1992; Nightingale et al., 2000). Wind speed is a parameter that is easy to measure and captures much of the variability in the turbulence at the air-sea exchange interface. The mass transfer coefficient K_w (cm h^{-1}) is calculated by Eq. (3) according to Wanninkhof (1992). This is the most widely accepted method for determining wind-induced gas exchange fluxes, and is used extensively to estimate the air-sea Hg^0 exchange (Wangberg et al., 2001; Rolfhus and Fitzgerald, 2001),

$$K_w = 0.31 \cdot u_{10^2} \left(\frac{Sc_{Hg}}{660} \right)^{-0.5} \quad (3)$$

where u_{10} is the wind speed (m s^{-1}) 10 m above the sea surface, Sc_{Hg} is the Schmidt number of Hg^0 and 660 corresponds to the Schmidt number for CO_2 in seawater at 20 °C (Wanninkhof, 1992). In-turn, the Schmidt number for Hg^0 is derived from its definition as follows:

$$Sc_{Hg} = \frac{\nu}{D} \quad (4)$$

where ν is the kinematic viscosity (cm^2 s^{-1}) of seawater and D is the Hg^0 diffusion coefficient (cm^2 s^{-1}) in seawater, which was calculated

by the simulation of molecular dynamics, as described by Kuss et al. (2009). The kinematic viscosity of seawater at the desired temperature was calculated according to the method described by Wanninkhof (1992). In our calculations, we used a Sc_{Hg} value of 689, as proposed by Kuss et al. (2009) for seawater at $T = 20$ °C.

To apply the model, the measured wind speed at 2 m above the sea surface was corrected to u_{10} using the equation reported hereafter (Schwarzenbach et al., 1993),

$$u_{10} = \frac{10.4 u_z}{\ln(z) + 8.1} \quad (5)$$

where u_z is the wind speed (m s^{-1}) measured at the height z meters above the sea surface.The calculated evasional fluxes of Hg^0 are listed in Table 6, together with a summary of the DGM in the surface waters, the GEM in the air, the wind speed at the height of 10 m above sea level (u_{10}) and saturation in the investigated area offshore of Panarea.

Based on our DGM and GEM data and the two-layer gas exchange model at the air-seawater interface, the calculated average Hg^0 flux during the entire cruise campaign was $\sim 4.5 \pm 3.5$ ng m^{-2} h^{-1} (range: 0.7–9.1 ng m^{-2} h^{-1}; Table 6). Given the uncertainties associated with these models, we compared our evasional Hg^0 flux data estimated by the Wanninkhof (1992) parametrization with those resulted by the Nightingale et al. (2000) model. We found a strong positive correlation ($r^2 = 0.999$) between the obtained results (as listed in Table 6), suggesting that both models may be likely equivalent, at some extent.

A summary of the observed mercury fluxes presented in the literature in conjunction with the averaged data flux from this study is presented in Table 7. Our data on Hg^0 flux fall within the range proposed by Andersson et al. (2007) for the Mediterranean Sea (Table 7). Although Panarea is an important natural source of Hg from geotectonic activity (hydrothermal) compared to the main open oceans, similar Hg^0 flux values were reported in literature for the Pacific Ocean (3 ng m^{-2} h^{-1}, Kim and Fitzgerald, 1986; Mason and Fitzgerald, 1993), the North Atlantic Ocean (0.4 ± 0.3 ng m^{-2} h^{-1}, Andersson et al., 2011), the Arctic Ocean (2.4 ng m^{-2} h^{-1}, Andersson et al., 2008), the Baltic Sea (0.8–1.6 ng m^{-2} h^{-1}, Wangberg et al., 2001), the North Sea (0.2 to 4.6 ng m^{-2} h^{-1}, Baeyens and Leermakers, 1998), and for some polluted marine areas, such as Tokyo Bay (5.8 ± 5.0 ng m^{-2} h^{-1}, Narukawa et al., 2006), Minamata Bay (5 ± 5.8 ng m^{-2} h^{-1}, Marumoto et al., 2015), the Yellow Sea (0.88 ± 1.38 ng m^{-2} h^{-1}, Ci et al., 2011) and the Northern South China Sea (4.5 ng m^{-2} h^{-1}, Fu et al., 2010). This inconsistent analogy with the other marine areas may suggest that our Hg^0 flux calculated by the two-layer gas exchange model at Panarea has been likely underestimated due to the data gap concerning the role of the rising hydrothermal bubbles in transporting Hg from the submarine discharging vent (see Section 3.5.3). Of course, more research is needed to improve knowledge of the implications of gas bubbles as carrier for Hg^0 transport in submarine hydrothermal systems, representing a productive theme of inquiry for future studies. If we extend our calculations over the entire submarine degassing area of Panarea Island (~ 2.3 km^2), we obtain a total Hg^0 evasion flux of about 0.0001 t y^{-1}. Compared to a general overview of the results provided in the literature, this value accounts for a slight proportion of the total Hg flux released annually into the atmosphere from the entire Mediterranean Basin, accounting for 60–77 t y^{-1} (Andersson et al., 2007; Gardfeldt et al., 2003; Ferrara et al., 2000). Despite this, however, this study provides new important information with which to expand the currently limited database on Hg released from submarine hydrothermal activity, and allows some inferences to be made regarding the quality of previous estimates of mass balance for the Mediterranean Sea. Besides, because the annual Hg mass balance established for the Mediterranean Basin shows that exchanges with the atmosphere are the most important source/sink of mercury for the water compartment (Rajar et al., 2007; Žagar et al., 2007, 2014), our preliminary results suggest that emissions from submarine hydrothermal activity could instead represent an important local source of mercury for this region. A critical assessment of the published literature highlights that the previous mass balance promoting the average total natural submarine Hg emissions in the Mediterranean Sea of ~ 15 t y^{-1} (Rajar et al., 2007; Žagar et al., 2014), is an under-estimate. This is because studies on Hg abundance in the submarine hydrothermal discharge affecting the Basin and its dependence on environmental factors have so far not been considered in the modelling.

Compared to the volcanic flux from subaerial continuous passive degassing occurring in the Mediterranean region, mainly represented by Mt. Etna, Stromboli and Vulcano island, Hg^0 evasion flux from the submarine degassing system of Panarea appears less important. These three active volcanoes, in fact, account for a cumulative atmospheric Hg^0 flux of about 5.4 t y^{-1} under quiescence degassing activity (Bagnato et al., 2011, 2014). Nevertheless, although comprising a marginal contribution to the global volcanic non-eruptive Hg emissions, these new data represent the first available assessment of Hg^0 emissions directly sampled at these locations.

Table 7
Summary of observed mercury fluxes presented in the literature in conjunction with averaged data flux from this study.

Location	Flux (ng m^{-2} h^{-1})	References
Equatorial Pacific Ocean	1.1–5.4	Kim and Fitzgerald, 1986
Pacific Ocean	3	Kim and Fitzgerald, 1986; Mason and Fitzgerald, 1993
Arctic Ocean	2.4	Andersson et al., 2008
Entire North Sea	0.9–1.8	Coquery and Cossa, 1995
Southern North Sea	0.2–4.6	Baeyens and Leermakers, 1998
Scheldt Estuary, Belgium	2–4.9	Baeyens and Leermakers, 1998
North Atlantic Ocean	5–26.7	Mason et al., 1998
North Atlantic Ocean	0.1–0.7	Andersson et al., 2011
Baltic Sea	0.8–1.6	Wangberg et al., 2001
Mediterranean Sea	15	Gardfeldt et al., 2003
Mediterranean Sea	0.8–5.2	Andersson et al., 2007
Tokyo Bay, Japan	0.8–10	Narukawa et al. 2006
Minamata Bay, Japan	5 ± 5.8	Marumoto and Imai, 2015
Yellow Sea, China	0.88 ± 1.38	Ci et al., 2011
Northern South China Sea	4.5	Fu et al., 2010
Panarea submarine hydrothermal area	4.5 ± 3.5	This work

3.5.3. Uncertainties in the Hg^0 flux estimate

When comparing different works on estimating the air-water Hg^0 flux, it is important to bear in mind that the estimated Hg^0 flux using the two-layer gas exchange model is influenced by the choice of gas transfer parameterizations (K_w) and the diffusion coefficient of Hg^0 (Rolfhus and Fitzgerald, 2001; Andersson et al., 2007; Ci et al., 2011). As reviewed by Wanninkhof (1992), except for wind speed, several factors, such as bubbles, can influence K_w. The release of gas from a bubble into the atmosphere completes the process of air-sea gas exchange mediated by the rising bubbles (Farmer et al. 1993; Erickson 1993). Several attempts have been made to predict the relative importance of gas exchange and bubble processes on gas supersaturation (Merlivat and Memery, 1983; Woolf and Thorpe, 1991; Woolf, 1993), but evaluating the bubble-mediated gas exchange flux is complicated by uncertainties over the bubble number density, volume concentrations and depth distributions (Upstill-Goddard, 2006). The gas partial pressure inside ocean surface bubbles is generally higher than the partial pressure of the same gases in the atmosphere. This is because hydrostatic pressure and surface curvature contribute a significant extra pressure inside the gas bubbles. Gas transfer mediated by bubbles is more efficient than the transfer through the air-sea interface (Zhang, 2012). Very small bubbles (< 0.005 cm) that are injected into deep water can completely collapse under hydrostatic pressure, meaning that

their entire contents are dissolved into the water and never reach the surface (Craig and Weiss, 1971; Zhang, 2012). For large bubbles, gas exchange continues until bubbles reach the water surface (Fuchs et al., 1987; Woolf, 1993). The two-layer gas exchange model used in this study to estimate the Hg^0 emission rate does not include the contribution of rising hydrothermal bubbles. To address this data gap, we performed preliminary *in-situ* Hg^0 flux estimates at the sea-air interface using the floating accumulation chamber methodology, which is widely employed elsewhere (Bagnato et al., 2013; Wang et al., 2006; Gardfeldt et al., 2003; Covelli et al., 1999; Kim and Lindberg, 1995; Zhang and Lindberg, 2001). Using this approach, we measured a cumulative flux provided by the sum of both the diffusive evasional flux from the dissolved Hg phase in surface seawater (DGM) and the bubble-mediated gas component. In order to ensure optimal sampling conditions (i.e. low wind speed and absence of waves), Hg evasional flux measurements using the flux chamber technique were only performed at the BN station, which is the shallowest vent site where a strong rising gas bubbling plume was clearly visible at the sea surface during the survey. At this site, the gas flux at the sea-air surface was calculated based on the rate of concentration increases in the chamber using the following theoretical equation:

$$\Phi = c_f \times \frac{dC}{dt} \quad (6)$$

where Φ is the flux of a gas, dC/dt is the rate of concentration change in the accumulation chamber air for each investigated gas, and c_f is a proportionality factor that, theoretically, is provided by the ratio between the volume of the chamber and the surface area at the bottom of the chamber (Chiodini et al., 1998). These measurements gave an Hg^0 evasional flux of about 8 ng m^{-2} h^{-1}, which was up to 10 times greater than the value obtained by the model (Table 6). This confirms the importance of the bubble-mediated gas exchange flux in estimating the total Hg^0 emission rate at the sea-air interface from the submarine thermal outgassing. By comparing this additional information with the results obtained by the model and previous Hg^0 flux determinations in the Mediterranean Sea (Table 7), we can propose that 1) the data obtained by the floating accumulation flux chamber technique at BN seem very reasonable; 2) in a scenario like that encountered at Panarea island, a great deal of the uncertainty in the traditional relationship of the gas transfer velocity for estimating the Hg^0 evasional flux by the gas-exchange model may be ascribed to the neglect of the breaking hydrothermal bubbles effect at the sea-air interface; and 3) the use of the two-layer gas-exchange model to estimate the atmospheric evasive Hg^0 flux from the submarine hydrothermal degassing could have underestimated the calculation to some extent.

4. Conclusions

On a cruise campaign carried out in 2015 in the Mediterranean Sea (15–17th June and 17–18th November), we investigated the concentrations of Hg species in hydrothermal fluids vented from the submarine exhalative area of Panarea Island. The use of a natural laboratory like Panarea, where hydrothermally produced Hg and other major gases (such as CO_2 and H_2S) leak from the seafloor into the overlying water column has enabled us to examine the vertical distribution and temporal impact of these gases on marine chemistry and test new technologies for monitoring the escape of Hg species. The impact of the leaks on the marine environment is clearly visible in the area, but with very local effects. The spatial distribution of FTHg and RHg with depth showed no significant water column variations, probably due to the dilution operated by the efficient currents that mix vertically and make the column uniform. Anyway, more studies are needed to better define these effects. Conversely, the FTHg content in the hydrothermal fluids showed a clear difference from the water column over the vents. The small RHg/FTHg ratio measured in the fluids suggests that part of RHg in the submarine hydrothermal systems is probably involved in reducing biotic mechanisms in order to produce DGM form. The DGM and the GEM were measured simultaneously during the cruise and combined in a gas-exchange model to calculate the sea-air Hg^0 evasional flux. The averaged Hg^0 flux of $\sim 4.5 \pm 3.5$ ng m^{-2} h^{-1}, which was calculated at Panarea by the model, is analogous to previous values proposed by many authors for the Mediterranean Sea. Given the various sources of uncertainty in models designed to assess Hg^0 air-sea exchange, the time-averaged Hg^0 flux from the submarine hydrothermal activity at Panarea is likely even larger if the bubbles contribution is considered. This area, however, should continue to be a productive theme of inquiry for future studies. Further measurement campaigns are needed in order to perform more detailed studies on the parameters influencing mercury evasion at different locations of the Mediterranean Sea such as the season and solar radiation. The complicated cycling of Hg in the marine environment indicates that short-term field observation cannot capture the integrated figure of the mercury cycle. In spite of this, and although the water surface off-shore area of Panarea Island represents only a small part of the total oceanic surfaces on the Earth, we believe that the results presented in this study may be of help in improving the global mercury budget and cycle, since such measurements in large parts of the world's marine environments are still lacking.

Acknowledgements

This research is part of the MONSOON research program, funded by the Assessorato Regionale delle Attività Produttive (Regione Siciliana), who we gratefully acknowledge. The authors wish to thank the crew of R/V Bio 4 You for their valuable professionalism and support during the oceanographic cruises, and in particular Dr. Gaspare Buffa of IAMCCNR (Capo Granitola). We acknowledge Drs. Cinzia Giuseppina Caruso and Alessandra Nigrelli for their local assistance. We are very grateful to Francesco Salerno and Vincenzo Prano for Gas Chromatography (GC) and Ion Chromatography (IC) analysis at INGV-Palermo (Italy). Finally, our measurements at the submarine hydrothermal system of Panarea Island would not have been possible without the expertise in diving of Dr. Carlo Patti of IAMC-CNR (Capo Granitola), who sampled both submarine thermal fluids and seawater. The authors also wish to thank the Editor, and the Reviewers for their fruitful comments on an earlier version of the manuscript.

References

Aiuppa, A., Bagnato, E., Witt, M.L.I., Mather, T.A., Parello, F., Pyle, D.M., Martin, R.S., 2007. Real-time simultaneous detection of volcanic Hg and SO_2 at La Fossa Crater, Vulcano (Aeolian Islands, Sicily). Geophys. Res. Lett. 34, L21307.

Amyot, M., Gill, G.A., Morel, F.M.M., 1997. Production and loss of dissolved gaseous mercury in coastal seawater. Environ. Sci. Technol. 31, 3606–3611.

Andaloro, F., Romeo, T., Renzi, M., Guerranti, C., Perra, G., Consoli, P., Perzia, P., Focardi, S.E., 2012. Alteration of potential harmful elements levels in sediments and biota from the central Mediterranean Sea (Aeolian Archipelago) following an episode of intense volcanic activity. Environ. Monit. Assess. 184, 4035.

Andersson, M.E., Gardfeldt, K., Wangberg, I., Sprovieri, F., Pirrone, N., Lindqvist, O., 2007. Seasonal and daily variation of mercury on and off shore sites from the Mediterranean Sea. Mar. Chem. 107 (1), 104–116.

Andersson, M.E., Gardfeldt, K., Wangberg, I., Stromberg, D., 2008. Determination of Henry's law constant for elemental mercury. Chemosphere 73, 587–592.

Andersson, M.E., Sommar, J., Gardfeldt, K., 2011. Air–sea exchange of volatile mercury in the North Sea. Mar. Chem. 125, 1–7.

Asthakhov, A.S., Koruykin, G.I., Ivanov, M.V., 2005. Nature mercury emission from Earth Crust in Artic and subartic marine environ ments. Geophys. Res. Abstr., vol. 7, 649 (European Geosciences Union).

Astakhov, A.S., Wallmann, K., Ivanov, M.V., Kolesov, G.M., Sattarova, V.V., 2007. Distribution and accumulation rate of Hg in the Upper Quaternary sediments of the Deryugin Basin, Sea of Okhotsk. Geochem. Int. 45 (1), 47–61.

Astakhov, A.S., Ivanov, M.V., Li, B.Y., 2011. Hydrochemical and atmochemical mercury dispersion zones over hydrothermal vents of the submarine Piip Volcano in the Bering Sea. Oceanology 51, 826.

Baeyens, W., Leermakers, M., 1998. Elemental mercury concentrations and formation rates in the Scheldt estuary and the North Sea. Mar. Chem. 60, 257–266.

Bagnato, E., Aiuppa, A., Parello, F., Allard, P., Liuzzo, M., Giudice, G., Shinohara, H., 2011. New clues on mercury contribution from Earth volcanism. Bull. Volcanol. 73,

497–510.
Bagnato, E., Sprovieri, M., Barra, M., Bitetto, M., Bonsignore, M., Calabrese, S., Di Stefano, V., Oliveri, E., Parello, F., Mazzola, S., 2013. The sea-air exchange of mercury (Hg) in the marine boundary layer of the Augusta basin (southern Italy): concentrations and evasion flux. Chemosphere 93 (9), 2024–2032.
Bagnato, E., Tamburello, G., Avard, G., Martinez, M., Enrico, M., Fu, X., Sprovieri, M., Sonke, J., 2014. Mercury fluxes from volcanic and geothermal sources: an update. In: The Role of Volatiles in the Genesis, Evolution and Eruption of Arc Magmas. Edited by Geological Society of London; available online http://sp.lyellcollection.org/; doi http://dx.doi.org/10.1144/SP410.2.
Barnes, H.L., 1979. Geochemistry of Hydrothermal Ore Deposits, 2° edition. John Wiley Editor, New York.
Caliro, S., Caracausi, A., Chiodini, G., Ditta, M., Italiano, F., Longo, M., Minopoli, C., Nuccio, P.M., Paonita, A., Rizzo, A., 2004. Evidence of a recent input of magmatic gases into the quiescent volcanic edifice of Panarea, Aeolian Islands, l Italy. Geophys. Res. Lett. 31, L07619. http://dx.doi.org/10.1029/2003GL019359.
Caracausi, A., Ditta, M., Italiano, F., Longo, M., Nuccio, P.M., Paonita, A., Rizzo, A., 2005. Changes in fluid geochemistry and physico-chemical conditions of geothermal systems caused by magmatic input: the recent abrupt outgassing off the island of Panarea (Aeolian Islands, Italy). Geochim. Cosmochim. Acta 69 (12), 3045–3059.
Caramanna, G., Voltattorni, N., Caramanna, L., Cinti, D., Galli, G., Pizzino, L., Quattrocchi, F., 2005. Scientific diving techniques applied to the geomorphological and geochemical study of some submarine volcanic gas vents (Aeolian Islands-Southern Tyrrhenian Sea-Italy). In: Diving for Science: Proceedings of the 24th Symposium of American Academy of Underwater Sciences.
Caramanna, G., Espa, S., Bouché, V., 2010. Study of the environmental effects of submarine CO_2-rich emissions by means of scientific diving techniques (Panarea Island-Italy). Int. J. Soc. Underwater Technol. 29 (2), 79–85.
Carr, R.A., Jones, M.M., Warner, T.B., Cheek, C.H., Russ, E.R., 1975. Variation in time of mercury anomalies at the Mid-Atlantic Ridge. Nature 258, 588–589.
Chiodini, G., Cioni, R., Guidi, M., Raco, B., Marini, L., 1998. Soil CO_2 flux measurements in volcanic and geothermal areas. Appl. Geochem. 13 (5), 543–552.
Ci, Z.J., Zhang, X.S., Wang, Z.W., Niu, Z.C., Diao, X.Y., Wang, S.W., 2011. Distribution and air–sea exchange of mercury (Hg) in the Yellow Sea. Atmos. Chem. Phys. 11, 2881–2892.
Coquery, M., Cossa, D., 1995. Mercury speciation in surface waters of the North Sea. Neth. J. Sea Res. 34, 245–257.
Cossa, D., Coquery, M., 2005. The Mediterranean mercury anomaly, a geochemical or a biological issue. In: Hdb. Env. Chem. 5. Springer-Verlag, Heidelberg.
Cossa, D., Martin, J.M., Takayanagi, K., Sanjuan, J., 1997. The distribution and cycling of mercury species in the western Mediterranean. Deep-Sea Res. II 44, 721–740.
Costa, M., Liss, P.S., 1999. Photoreduction of mercury in sea water and its possible implications for Hg0 air–sea fluxes. Mar. Chem. 68, 87–95.
Costa, M., Liss, P.S., 2000. Photoreduction and evolution of mercury from seawater. Sci. Total Environ. 261, 125–135.
Covelli, S., Faganeli, J., Horvat, M., Brambati, A., 1999. Porewater distribution and benthic flux measurements of mercury and methylmercury in the gulf of Trieste (Northern Adriatic Sea). Estuar. Coast. Shelf Sci. 48, 415–428.
Craig, H., Weiss, R., 1971. Dissolved gas saturation anomalies and excess helium in the ocean. Earth Planet. Sci. Lett. 10, 289–296.
Cronan, D.S., 1972. The mid-Atlantic Ridge near 45°N: Al, As, Hg, and Mn in ferruginous sediments from the median valley. Can. J. Earth Sci. 9, 319–323.
Dalziel, J.A., 1995. Reactive mercury in eastern North Atlantic and Southern Atlantic. Mar. Chem. 49, 307–314.
D'Asaro, E., McNeil, C., 2007. Air-sea gas exchange at extreme wind speeds measured by autonomous oceanographic floats. J. Mar. Syst. 66, 92–109.
Dekov, V.M., 2007. Native Hgliq in the metalliferous sediments of the East Pacific Rise (21°S). Mar. Geol. 238, 107–113.
Dekov, V.M., Savelli, C., 2004. Hydrothermal activity in the SE Tyrrhenian Sea: an overview of 30 years of research. Mar. Geol. 204, 161–185.
Erickson, D.J., 1993. A stability dependent theory for air-sea gas exchange. J. Geophys. Res. 98, 8471–8488.
Fantozzi, L., Ferrara, R., Frontini, F.P., Dini, F., 2007. Factors influencing the daily behaviour of dissolved gaseous mercury concentration in the Mediterranean Sea. Mar. Chem. 107, 4–12.
Fantozzi, L., Ferrara, R., Frontini, F.P., Dini, F., 2009. Dissolved gaseous mercury production in the dark: evidence for the fundamental role of bacteria in different types of Mediterranean water bodies. Sci. Total Environ. 407, 917–924.
Fantozzi, L., Manca, G., Ammoscato, I., Pirrone, N., Sprovieri, F., 2013. The cycling and sea–air exchange of mercury in the waters of the Eastern Mediterranean during the 2010 MED-OCEANOR cruise campaign. Sci. Total Environ. 448, 151–162.
Farmer, D.M., McNeil, C.L., Johnson, B.D., 1993. Evidence for the importance of bubbles in increasing air-sea gas flux. Nature 361, 620–623.
Ferrara, R., Mazzolai, B., Lanzillotta, E., Nucaro, E., Pirrone, N., 2000. Temporal trends in gaseous mercury evasion from the Mediterranean seawaters. Sci. Total Environ. 259, 183–190.
Ferrara, R., Lanzillotta, E., Ceccarini, C., 2001. Dissolved gaseous mercury concentration and mercury evasional flux from seawater in front of a chlor-alkali plant. Environ. Technol. 22 (8), 971–978.
Ferrara, R., Ceccarini, C., Lanzillotta, E., Gardfeldt, K., Sommar, J., Horvat, M., Logar, M., Fajon, V., Kotnik, 2003. Profiles of dissolved gaseous mercury concentration in the Mediterranean seawater. Atmos. Environ. 37, 85–92.
Fitzgerald, W.F., Lamborg, C.H., Hammerschmidt, C.R., 2007. Marine biogeochemical cycling of mercury. Chem. Rev. 107, 641–662.
Fu, X.W., Feng, X.B., Zhang, G., Xu, W.H., Li, X.D., Yao, H., Liang, P., Li, J., Sommar, J., Yin, R., Liu, N., 2010. Mercury in the marine boundary layer and seawater of the South China Sea: concentrations, sea/air flux, and implication for land outflow. J. Geophys. Res. 115, D06303.
Fuchs, G., Roether, E.W., Schlosser, P., 1987. Excess 3He in the ocean layer. J. Geophys. Res. 92, 6559–6568.
Gabbianelli, G., Gillot, P.Y., Lanzafame, G., Ligi, M., Postpisch, D., Rossi, P.L., 1986. Controllo strutturale nell'evoluzione vulcanica di Panarea (Isole Eolie). In: CNR IIV Open File Rep. 4/86, pp. 27.
Gårdfeldt, K., Feng, X., Sommar, J., Lindqvist, O., 2001. Total gaseous mercury exchange between air and water at river and sea surfaces in Swedish coastal regions. Atmos. Environ. 35, 3027–3038.
Gardfeldt, K., Sommar, J., Ferrara, R., Ceccarini, C., Lanzillotta, E., Munthe, J., Wangberg, I., Lindqvist, O., Pirrone, N., Sprovieri, F., Pesenti, E., Stromberg, D., 2003. Evasion of mercury from coastal and open waters of the Atlantic Ocean and the Mediterranean Sea. Atmos. Environ. 37 (1), S73–S84 Supplement No.
Gasparini, P., Iannaccone, G., Scandone, P., Scarpa, R., 1982. The seismotectonics of the Calabrian Arc. Tectonophys. 84, 267–286.
Gugliandolo, C., Italiano, F., Maugeri, T.L., 2006. The submarine hydrothermal system of Panarea (Southern Italy): biogeochemical processes at the thermal fluids-sea bottom interface. Ann. Geophys. 49, 783–792.
Gustin, M.S., Lindberg, S., Marsik, F., Casimir, A., Ebinghaus, R., Edwards, G., Hubble-Fitzgerald, C., Kemp, R., Kock, H., Leonard, T., London, J., Majewski, M., Montecinos, C., Owens, J., Pilote, M., Poissant, L., Rasmussen, P., Schaedlich, F., Schneeberger, D., Schroeder, W., Sommar, J., Turner, R., Vette, A., Wallschlaeger, D., Xiao, Z., Zhang, H., 1999. Nevada STORMS project: measurement of mercury emissions from naturally enriched surfaces. J. Geophys. Res. 104, 21831–21844.
Hamme, R.C., Emerson, S.R., 2002. Mechanisms controlling the global oceanic distribution of the inert gases argon, nitrogen and neon. Geophys. Res. Lett. 29 (23), 2120. http://dx.doi.org/10.1029/2002GL015273.
Hamme, R.C., Emerson, S.R., 2006. Constraining bubble dynamics and mixing with dissolved gases: Implications for productivity measurements by oxygen mass balance. J. Mar. Res. 64, 73–95.
Horvat, M., Kotnik, J., Logar, M., Fajon, V., Zvonaric, T., Pirrone, N., 2003. Speciation of mercury in surface and deep-sea waters in the Mediterranean Sea. Atmos. Environ. 37, 93–108.
Inguaggiato, S., Italiano, F., 1998. Helium and carbon isotopes in submarine gases from the Aeolian arc (Southern Italy). In: Proceeding of the 9th International Symposium on Water-Rock Interaction-WRI9, 30 March-3 April 1998, pp. 727–730 Taupo, New Zealand (Arehart & Hulston, Rotterdam).
Italiano, F., Nuccio, P.M., 1991. Geochemical investigations on submarine volcanic exhalations to the East of Panarea, Aeolian Islands, Italy. J. Volcanol. Geotherm. Res. 46, 125–141.
Khodakovskiy, I.L., Shikina, N.D., 1983. The role of carbonate complexes in mercury transport in hydrothermal solutions (experimental studies and thermodynamic analysis). Geochem. Int. 18 (3), 32–43.
Kim, J.P., Fitzgerald, W.F., 1986. Sea-air partitioning of mercury in the equatorial Pacific Ocean. Science 28, 1131–1133.
Kim, K.H., Lindberg, S., 1995. Design and initial tests of dynamic enclosure chamber for measurements of vapour-phase mercury fluxes over soils. Water Air Soil Pollut. 80, 1059–1068.
Kim, K.H., Mishra, V.K., Hong, S., 2006. The rapid and continuous monitoring of gaseous elemental mercury (GEM) behavior in ambient air. Atmos. Environ. 40, 3281–3293.
Kotnik, J., Horvat, M., Tessier, E., Ogrinc, N., Monperrus, M., Amouroux, D., Fajon, V., Gibičar, D., Žižek, S., Sprovieri, F., Pirrone, N., 2007. Mercury speciation in surface and deep waters of the Mediterranean Sea. Mar. Chem. 107 (1), 13–30.
Kotnik, J., Sprovieri, F., Ogrinc, N., Horvat, M., Pirrone, N., 2013. Mercury in the Mediterranean. Part 1: spatial and temporal trends. Environ. Sci. Pollut. Res. http://dx.doi.org/10.1007/s11356-013-2378-2.
Krauskopf, K.B., 1951. Physical chemistry of quicksilver tansportation in vein fluids. Econ. Geol. 46, 498–523.
Krupp, R., 1988. Physicochemical aspects of mercury metallogenesis. Chem. Geol. 69, 345–356.
Kuss, J., Holzmann, J., Ludwig, R., 2009. An elemental mercury diffusion coefficient for natural waters determined by molecular dynamics simulation. Environ. Sci. Technol. 43, 3183–3186.
Lamborg, C.H., Von Damm, K.L., Fitzgerald, W.F., Hammerschmidt, C.R., Zierenberg, R.A., 2006. Mercury and monomethylmercury in fluids from Sea Cliff submarine hydrothermal field, Gorda Ridge. Geophys. Res. Lett. 33, L17606.
Lamborg, C.H., Yigiterhan, O., Fitzgerald, W.F., Balcom, P.H., Hammerschmidt, C.R., Murray, J.W., 2008. Vertical distribution of mercury species at two sites in the western Black Sea. Mar. Chem. 111, 77–89.
Langmuir, D., 1977. Aqueous Environmental Geochemistry. Prentice Hall, New Jersey, pp. 600.
Lanzillotta, E., Ferrara, R., 2001. Daily trend of dissolved gaseous mercury concentration in coastal seawater of the Mediterranean basin. Chemosphere 45, 935–940.
Lanzillotta, E., Ceccarini, C., Ferrara, R., 2002. Photo-induced formation of dissolved gaseous mercury in coastal and offshore seawater of the Mediterranean basin. Sci. Total Environ. 300, 179–187.
Laurier, F.J.G., Mason, R.P., Gill, G.A., Whalin, L., 2004. Mercury distributions in the North Pacific Ocean-20 years of observations. Mar. Chem. 90 (1–4), 3–19.
Liss, P.S., 1983. Gas transfer: experiments and geochemical implications. In: Liss, P.S., Slinn, W.G.N. (Eds.), Air -sea exchange of gaseous and particles. NATO ASI Series, D. Reidel Publishing Company, Dordrecht, Boston, Lancaster, pp. 241–259.
Liss, P.W., Slater, P.G., 1974. Flux of gases across the air-sea interface. Nature 247, 181–184.
Marumoto, K., Imai, S., 2015. Determination of dissolved gaseous mercury in seawater of Minamata Bay and estimation for mercury exchange across air–sea interface. Mar.

Chem. 168, 9–17.
Mason, R.P., Fitzgerald, W.F., 1990. Alkylmercury in the equatorial Pacific. Nature 374, 457–459.
Mason, R.P., Fitzgerald, W.F., 1993. The distribution and biogeochemical cycling of mercury in the equatorial Pacific Ocean. Deep-Sea Res. 40, 1897–1907.
Mason, R.P., Sheu, G.R., 2002. Role of the ocean in the global mercury cycle. Glob. Biogeochem. Cycles 16 (4), 1093. http://dx.doi.org/10.1029/2001GB001440.
Mason, R.P., Sullivan, K.A., 1999. The distribution and speciation of mercury in the South and equatorial Atlantic. Deep-Sea Res. II Top. Stud. Oceanogr. 46 (5), 937–956.
Mason, R.P., Fitzgerald, W.F., Morel, F.M.M., 1994. The biogeochemical cycling of elemental mercury: anthropogenic influences. Geochim. Cosmochim. Acta 58, 3191–3198.
Mason, R.P., Rolfhus, K.R., Fitzgerald, W.F., 1995. Methylated and elemental mercury cycling in surface and deep-ocean waters of the North Atlantic. Water Air Soil Pollut. 80, 665–667.
Mason, R.P., Rolfhus, K.R., Fitzgerald, W.F., 1998. Mercury in the North Atlantic. Mar. Chem. 61, 37–53.
McDougall, T.J., 1978. Bubble plumes in stratified environments. J. Fluid Mech. 85 (Issue 4), 655–672.
Merlivat, L., Memery, L., 1983. Gas exchange across an air–water interface: experimental results and modeling of bubble contribution to transfer. J. Geophys. Res. 88 (C1), 707–724.
Morel, F.M.M., Kraepiel, A.M.L., Amyot, M., 1998. The chemical cycle and bioaccumulation of mercury. Annu. Rev. Ecol. Syst. 29, 543–566.
Narukawa, M., Sakata, M., Marumoto, K., Asakura, K., 2006. Air-sea exchange of mercury in Tokyo Bay. J. Oceanogr. 62, 249–257.
Nightingale, P.D., Malin, G., Law, C.S., Watson, A.J., Liss, P.S., Liddicoat, M.I., Boutin, J., Upstill-Goddard, R.C., 2000. In situ evaluation of air–sea gas exchange parameterizations using novel conservative and volatile tracers. Global Biogeochem. Cycles 14 (1), 373–387.
Panieri, G., Gamberi, F., Marani, M., Barbieri, R., 2005. Benthic foraminifera from a recent, shallow-water hydrothermal environment in the Aeolian Arc (Tyrrhenian Sea). Mar. Geol. 218, 207–229.
Parker, J.L., Bloom, N.S., 2005. Preservation and storage techniques for low-level aqueous mercury speciation. Sci. Total Environ. 337, 253–263.
Poulain, A.J., Ní Chadhain, S.M., Ariya, P.A., Amyot, M., Garcia, E., Campbell, P.G.C., Zylstra, G.J., Barkay, T., 2007. Potential for mercury reduction by microbes in the high Arctic. Appl. Environ. Microbiol. 73, 2230–2238.
Prol-Ledesma, R.M., Canet, C., Melgarejo, J.C., Tolson, G., Rubio-Ramos, M.A., Cruz-Ocampo, J.C., Ortega-Osorio, A., Torres-Vera, M.A., Reyes, A., 2002. Cinnabar deposition in submarine coastal hydrothermal vents, Pacific Margin of central Mexico. Econ. Geol. 97, 1331–1340.
Prol-Ledesma, R.M., Canet, C., Torres-Vera, M.A., Forrest, M.J., Armienta, M.A., 2004. Vent fluid chemistry in Bahı'a Concepcio'n coastal submarine hydrothermal system, Baja California Sur, Mexico. J. Volcanol. Geotherm. Res. 137, 311–328.
Qureshi, A., O'Driscoll, N.J., Macleod, M., Meuhold, Y., Hungerbuhler, K., 2010. Photoreactions of mercury in surface ocean water: gross reaction kinetics and possible pathways. Environ. Sci. Technol. 44, 644–649.
Rajar, R., Žagar, D., Horvat, M., Četina, M., 2007. Mass balance of mercury in the Mediterranean Sea. Mar. Chem. 107, 89–102.
Resing, J.A., Lupton, J.E., Feely, R.A., Lilley, M.D., 2004. CO_2 and ^3He in hydrothermal plumes: implications for mid-ocean ridge CO_2 flux. Earth Planet. Sci. Lett. 226, 449–464.
Rolfhus, K.R., Fitzgerald, W.F., 2001. The evasion and spatial/temporal distribution of mercury species in Long Island Sound CT-NY. Geochim. Cosmochim. Acta 65 (3), 407–418.
Rolfhus, K.R., Fitzgerald, W.F., 2004. Mechanisms and temporal variability of dissolved gaseous mercury production in coastal seawater. Mar. Chem. 90, 125–136.
Sakamoto, H., 1985. The distribution of mercury, arsenic and antimony in sediments of Kagoshima Bay. Bull. Chem. Soc. Jpn. 58, 580–587.
Sanemasa, I., 1975. The solubility of elemental mercury vapor in water. Bull. Chem. Soc. Jpn. 48, 1795–1798.
Sarkar, D., 2003. Preliminary studies on mercury solubility in the presence of iron oxide phases using static headspace analysis. Environ. Geosci. 10 (4), 151–155.
Schroeder, W.H., Munthe, J., 1998. Atmospheric mercury: an overview. Atmos. Environ. 32 (5), 809–822.
Schwarzenbach, R.P., Gashwend, P.M., Imborden, D.M., 1993. Environmental Organic Chemistry. Wiley Inter-science, New York, pp. 228.
Sholupov, S., Pogarev, S., Ryzhov, V., Mashyanov, N., Stroganov, A., 2004. Zeeman atomic absorption spectrometer RA-915þ for direct determination of mercury in air and complex matrix samples. Fuel Process. Technol. 85, 473–485.
Soerensen, A.L., Sunderland, E.M., Holmes, C.D., Jacob, D.J., Yantosca, R.M., Skov, H., Christensen, J.H., Strode, S.A., Mason, R.P., 2010. An improved global model for air-sea exchange of mercury: high concentrations over the North Atlantic. Environ. Sci. Technol. 44, 8574–8580.
Solomon, E.A., Kastner, M., MacDonald, I.R., Leifer, I., 2009. Considerable methane fluxes to the atmosphere from hydrocarbon seeps in the Gulf of Mexico. Nat. Geosci. 2, 561–565.
Steffen, A., Schroeder, T.W., Macdonald, R., Poissant, L., Konoplev, A., et al., 2005. Mercury in the Arctic atmosphere: An analysis of eight years of measurements of GEM at Alert (Canada) and a comparison with observations at Amderma (Russia) and Kuujjuarapik (Canada). Sci. Total Environ. 342, 185–198.
Steinbruckner, D., 2009. Quantification of submarine degassing of Panarea Volcano in the Aeolian archipelago, Italy. Freiberg Online Geology 23 (ISSN 1434-7512).
Tassi, F., Capaccioni, B., Caramanna, G., Cinti, C., Montegrossi, G., Pizzino, L., Quattrocchi, F., Vaselli, O., 2009. Low-pH waters discharging from submarine vents at Panarea Island (Aeolian Islands, southern Italy) after the 2002 gas blast: Origin of hydrothermal fluids and implications for volcanic surveillance. Appl. Geochem. 24, 246–254.
Tivey, M.K., 2007. Generation of seafloor hydrothermal vent fluids and associated mineral deposits. Oceanography 20 (1), 50–65 Number.
Tomiyasu, T., Eguchi, T., Yamamoto, M., Anazawa, K., Sakamoto, H., Ando, T., Nedachi, M., Marumo, K., 2007. Influence of submarine fumaroles on the distribution of mercury in the sediment of Kagoshima Bay. Japan. Mar. Chem. 107, 173–183.
Upstill-Goddard, R.C., 2006. Air-sea exchange in the coastal zone. Estuar. Coastal Shelf. Sci. 70, 388.
USEPA, 1997. An assessment of exposure to mercury in the United States. In: Mercury Study Report to Congress. vol. 4.
USEPA, 2002. Method 1631. In: Revision E: Mercury in Water by Oxidation, Purge and Trap, and Cold Vapor Atomic Fluorescence Spectrometry, (EPA-821-R-02-019, United States).
Vagle, S., McNeil, C., Steiner, N., 2010. Upper ocean bubble measurements from the NE pacific and estimates of their role in air-sea gas transfer of the weakly soluble gases nitrogen and oxygen. J. Geophys. Res. 115, C12054. http://dx.doi.org/10.1029/2009JC005990.
Varekamp, J.C., Buseck, P.R., 1984. The speciation of mercury in hydrothermal systems, with applications for ore deposition. Geochim. Cosmochim. Acta 48, 177–186.
Von Damm, K.L., Edmond, J.M., Grant, B., Measures, C.I., Walden, B., Weiss, R.F., 1985. Chemistry of submarine hydrothermal solutions at 21°N, East Pacific Rise. Geochim. Cosmochim. Acta 49, 2197–2220.
Wang, D., He, L., Shi, X., Wei, S., Feng, X., 2006. Release flux of mercury from different environmental surfaces in Chongqing, China. Chemosphere 64 (11), 1845–1854.
Wangberg, I., Schmolke, S., Schgar, P., Munthe, J., Ebinghaus, R., Iverfeldt, A., 2001. Estimates of air-sea exchange of mercury in the Baltic Sea. Atmos. Environ. 35, 5477–5484.
Wanninkhof, R., 1992. Relationship between wind speed and gas exchange over the ocean. J. Geophys. Res. 97 (C5), 7373–7382.
Woolf, D.K., 1993. Bubbles and the air-sea transfer velocity of gases. Atmosphere-Ocean 31 (4), 517–540.
Woolf, D.K., Thorpe, S.A., 1991. Bubbles and the air-sea exchange of gases in near-saturation conditions. J. Mar. Res. 49, 435–466.
Žagar, D., Petkovsek, G., Rajar, R., Sirnik, N., Horvat, M., Voudouri, A., Kallos, G., Cetina, M., 2007. Modelling of mercury transport and transformations in the water compartment of the Mediterranean Sea. Mar. Chem. 107, 64–88.
Žagar, D., Sirnik, N., Četina, M., Horvat, M., Kotnik, J., Ogrinc, N., Hedgecock, I.M., Cinnirella, S., De Simone, F., Gencarelli, C.N., Pirrone, N., 2014. Mercury in the Mediterranean. Part 2: processes and mass balance. Environ. Sci. Pollut. Res. 21, 4081–4094.
Zhang, X., 2012. Contribution to the global air-sea CO_2 exchange budget by asymmetric bubble-mediated gas transfer. Tellus B 64 (17), 260.
Zhang, H., Lindberg, S.E., 2001. Sunlight and iron(III)-induced photochemical production of dissolved gaseous mercury in freshwater. Environ. Sci. Technol. 35 (5), 928–935.